Environmental filtering shapes patch dynamics across isolated mesophotic reefs

Nicole C. Pittoors[1,2], Sarah M. Tweedt[3], Luke J. McCartin[1,2] , Samuel A. Vohsen[1,2,3], Luisa Lopera[4], Sophia Mihalek[5, 2], Jamie Lai[1], Kathleen Durkin[6,7], Lee Weigt[3], Marissa F. Nuttall[8,9], Annalisa Bracco[4,10], Christopher P. Meyer[3], Santiago Herrera[1,2,3*]

[1] Oceans Research Center, Lehigh University, Bethlehem, PA

[2] Department of Biological Sciences, Lehigh University, Bethlehem, PA

[3] National Museum of Natural History, Smithsonian Institution, Washington D.C.

[4] Georgia Institute of Technology, Atlanta, Georgia

[5] Texas A&M University, Corpus Christi, TX

[6] University of Washington, Seattle, WA

[7] Harvey Mudd College, Claremont, California

[8] Flower Garden Banks National Marine Sanctuary, Galveston, TX.

[9] Texas A&M University, Galveston, TX

[10] CMCC Foundation, Euro-Mediterranean Center on Climate Change, Milan, Italy

[*] Corresponding Author: santiago.herrera@lehigh.edu

Competing interests: The authors declare no competing interest.

ABSTRACT

Mesophotic coral ecosystems (MCEs; ~30–150 m) encompass vast but poorly characterized reef habitats. Using Autonomous Reef Monitoring Structures (ARMS), environmental DNA (eDNA), metabarcoding (COI, 18S), image analysis, and 1-km hydrodynamic models, we investigated the mechanisms structuring cryptobenthic metazoan communities across six mesophotic banks on the northwestern Texas–Louisiana continental shelf. Community composition was governed primarily by environmental filtering: depth and turbidity jointly explained nearly twice as much variance than geographic effects in ARMS metabarcoding datasets. Environmental distance predicted community dissimilarity up to tenfold better than geographic distance, and environmental coefficients were 5–15× larger than geographic ones in multiple regression models. Turbidity, shaped by the benthic nepheloid layer, was the dominant filter, influencing 57 % of COI phyla and 115 families in 18S data, favoring sediment-tolerant suspension feeders and excluding photoautotrophs. Depth effects, although significant, were weaker and taxon-specific. Hydrodynamic simulations revealed episodic, bidirectional connectivity among banks with low connection strengths, indicating variable but non-limiting dispersal. Residual spatial structure likely reflects stochastic dispersal and spatially structured habitat heterogeneity. Collectively, these results demonstrate that environmental filtering, dominated by turbidity, overrides dispersal limitation in shaping mesophotic cryptobenthic communities, identifying the nepheloid layer as a key physical driver linking shelf oceanography, biodiversity, and ecosystem function. Suspended particle dynamics associated with bottom nepheloid layers merit integration into conservation planning as important mediators of ecological connectivity in mesophotic and other patchy reef systems globally.

SIGNIFICANCE

Mesophotic coral ecosystems are globally understudied, especially with respect to biodiversity of cryptic communities. This study presents the first integrated biodiversity survey of its kind in mesophotic coral reef ecosystems, combining standardized colonization substrates (ARMS), metabarcoding, high-resolution imagery, historical records, and hydrodynamic modeling. Conducted across 336 km (181 nautical miles) of topographic features on the TX-LA continental shelf, this survey revealed hundreds of previously undocumented species. While modeled larval dispersal demonstrated connectivity between the features, we found that turbidity from the nepheloid layer acts as a dominant environmental filter, structuring benthic assemblages across spatial and depth gradients. These findings reshape our understanding of biodiversity distribution, dispersal limitation, and selective filtering in deep reef ecosystems, with broad implications for marine ecology and conservation.

INTRODUCTION

Mesophotic coral ecosystems (MCEs; ~30–150 m) are extensive but understudied components of coral reef seascapes (Lesser *et al.* 2009; Turner *et al.* 2017)). They may occupy an area comparable to or greater than that of shallow reefs, potentially comprising up to 80% of global coral reef habitat (Eyal *et al.* 2021; Montgomery *et al.* 2019; Pyle & Copus 2019). Recent calls to safeguard MCEs emphasize their contributions to biodiversity, fisheries, and ecological resilience, including depth-adapted and endemic assemblages that may be partially buffered from anthropogenic disturbances (Soares et al. 2020). Yet, fundamental gaps persist in characterizing MCE biodiversity and in resolving the connectivity that underpins ecosystem function across depths.

Cryptobenthic organisms, the small, often hidden organisms inhabiting reef interstices, represent one of the least explored components of MCEs. Globally, cryptofauna may comprise 30-60% of total reef biodiversity (Enochs 2012), contributing disproportionately to biomass and ecosystem function through detrital recycling, filtration, herbivory, and trophic transfer (Wolfe *et al.* 2020, 2023). Yet, their composition, diversity and ecological roles within MCEs remain virtually unknown, as most studies have focused on conspicuous macroinvertebrates and fishes (Ginsburg 1983; Reimer *et al.* 2019; Sanchez *et al.* 2023; Studivan & Voss 2018; Voss *et al.* 2014). Because cryptic taxa are easily overlooked by conventional SCUBA surveys, photo transects, and ROV imagery, uncovering this 'hidden majority' requires specialized sampling approaches and conceptual frameworks to explain biodiversity patterns across spatially discrete habitats shaped by environmental and dispersal processes.

Metacommunity theory provides a unifying framework for understanding how species interactions, dispersal, and environmental heterogeneity collectively structure ecological communities (Leibold *et al.* 2004). Originally articulated through four paradigms (patch dynamics, species sorting, mass effects, and the neutral perspective), subsequent empirical work has focused on quantifying the relative influence of environmental versus spatial processes on community composition (Cottenie 2005; Peres-Neto *et al.* 2006). Environmental filtering occurs when species distributions reflect habitat conditions and niche preferences, whereas dispersal limitation arises when colonization is constrained by geographic distance or barriers to exchange. The balance between these processes depends on spatial scale and habitat connectivity, with patch dynamics emphasizing colonization–extinction trade-offs in homogeneous environments (Holyoak *et al.* 2005) and species sorting highlighting deterministic niche-based assembly along environmental gradients (Fleming *et al.* 2022; Menegotto *et al.* 2019; Rodil *et al.* 2018).

Studies in deep marine systems reveal that community structure often reflects a complex interplay between environmental and dispersal forces. At broad oceanic scales, environmental niches may exert stronger control over species distributions (McClain *et al.* 2012; Meyer *et al.* 2016), whereas in

island-like habitats such as dropstones, local hydrodynamics and dispersal dynamics can more parsimoniously explain community assembly (Meyer *et al.* 2016). Along continental margins, both mechanisms interact to create mosaic biogeographic patterns (McClain *et al.* 2024). Metacommunity theory is particularly relevant to benthic marine habitats, where larval dispersal, habitat isolation, and environmental gradients jointly shape biodiversity (Cowen 2002; Heino *et al.* 2015; Mullineaux *et al.* 2018; Saeedi *et al.* 2022; Villalobos *et al.* 2024). Recent work on chemosynthetic and deep-sea coral communities has applied these paradigms to greater depths, revealing departures from classical expectations about dispersal limitation and environmental filtering (Cordes *et al.* 2025). Although metacommunity frameworks have been well established in shallow reef research and increasingly applied to deep-sea systems, the mesophotic zone remains comparatively understudied. With its intermediate depth range, patchy distribution, and pronounced environmental gradients, the mesophotic realm provides an exceptional natural laboratory for testing metacommunity principles. Historically, such efforts were constrained by limited sampling and taxonomic resolution, but recent advances in sampling, molecular, imaging, and modeling techniques now enable high-resolution analyses of community assembly, particularly for the cryptofauna that dominate mesophotic biodiversity.

The northwestern Texas–Louisiana continental shelf and slope form a mosaic of isolated hard-bottom outcrops rising from a predominantly muddy seafloor, spanning steep environmental and spatial gradients in depth, substrate, and hydrodynamics (Gardner *et al.* 1998; Rezak *et al.* 1985, 1990). Research in this region has documented diverse benthic assemblages, depth-stratified species distributions, and complex transitions from shallow to mesophotic zones (Aronson *et al.* 2005; Garavelli *et al.* 2018; Rezak *et al.* 1990; Studivan & Voss 2018). Oceanographic studies reveal dynamic circulation and mesoscale eddies that both facilitate and restrict larval exchange, generating variable connectivity among banks and along the continental margin (Limer *et al.* 2020; Lopera *et al.* 2025; Vasbinder *et al.* 2023). Population-genetic analyses further demonstrate species-specific connectivity regimes, ranging from well-connected taxa such as *Montastraea cavernosa* and *Lutjanus campechanus* (Studivan & Voss 2018; Zhou *et al.* 2024)) to others exhibiting fine-scale population structure and asymmetric dispersal (Galaska *et al.* 2021; Liu *et al.* 2021; Zhou *et al.* 2024). This combination of heterogeneous habitats, environmental gradients, and variable dispersal capabilites makes the region an ideal natural laboratory for testing how environmental filtering and dispersal limitation interact to structure mesophotic communities.

To test metacommunity theory with empirical data from MCEs, we employed a standardized, integrative approach to quantify cryptobenthic diversity and connectivity across environmental gradients on the northwestern Texas–Louisiana continental shelf. Specifically, we deployed Autonomous Reef Monitoring Structures (ARMS) across multiple banks and depths within the Flower Garden Banks region.

ARMS replicate the structural complexity of natural reef benthos using stacks of PVC settlement panels with alternating open and semi-closed layers, creating microhabitats that attract a broad range of sessile and motile species (Leray & Knowlton 2015; Zimmerman & Martin 2004).Their modular design enables passive colonization and standardized sampling of benthic communities over time. Following recovery, we applied DNA metabarcoding, to generate comprehensive inventories of eukaryotic diversity (Cristescu 2014; Hajibabaei *et al.* 2012). This approach provides an unprecedented view of cryptobenthic diversity and species turnover across mesophotic gradients, offering new insights into ecosystem structure, function, and resilience.

Here, we integrate ARMS-based metabarcoding and morphological analyses with environmental DNA (eDNA) from surrounding waters, in situ and satellite environmental data, and high-resolution (1 km) hydrodynamic particle-tracking models to address a central question in metacommunity ecology: Is community structure in isolated mesophotic reef systems primarily governed by environmental filtering or by dispersal limitation? If environmental filtering predominates, community similarity should align with environmental gradients irrespective of spatial distance. Conversely, if dispersal limitation dominates, similarity should track hydrodynamic connectivity among banks regardless of environmental differences. By combining standardized colonization substrates, molecular tools, environmental observations, and mechanistic dispersal modeling, this study provides a comprehensive, scale-aware assessment of mesophotic cryptobenthic diversity, turnover, and connectivity. Together, these analyses advance metacommunity theory and establish a framework for biodiversity monitoring,conservation and management in mesophotic coral ecosystems.

METHODS

Benthic Community Sampling

Thirty-six ARMS were deployed for two years across six topographic features (Stetson, East Flower Garden Bank, Bright, McGrail, Alderdice, and Diaphus) hosting coral reefs on the TX-LA continental shelf at depths of 54-85 m within the Coralline Algae Zone (**Fig. 1**). Triplicate sets of ARMS were positioned at ‘shallow’ coral habitats (54-66 m) and, where feasible, dual ‘deep’ locations (80-85 m), ensuring comprehensive sampling of habitat heterogeneity (**Fig S8**). Immediately prior to ARMS recovery, we collected eDNA water samples via 1.7L Niskin bottles mounted to the ROV *Global Explorer* according to detailed field methods found in (McCartin *et al.* 2024). ARMS units were then retrieved with the ROV *Global Explorer* using 45 µm mesh-lined crates to retain motile fauna. Each unit was held in chilled, filtered seawater until processing and then disassembled plate-by-plate following (Ransome *et al.* 2017). Plates were gently rinsed in filtered seawater; rinse water was sieved into three

fractions: >2 mm, 500 µm–2 mm, and 106–500 µm. All organisms >2 mm were sorted, counted, photographed, and preserved as voucher speciments; representatives of each morphospecies were selected for DNA barcoding, collectively forming the "2mm barcoded macrofauna" dataset. The two smaller fractions (hereafter "motile" 500 µm and 106 µm) were preserved in ethanol (95%), then decanted repeatedly to separate organic material from sediments; retained organics were homogenized and stored in 95% ethanol for DNA extraction. Each ARMS plate was photographed for quantitative image analysis; representative sessile organisms were subsampled as vouchers to provide genetic references, then all remaining sessile organisms were scraped and homogenized (the "sessile" fraction). To monitor potential contamination, filtered surface seawater from ARMS holding containers was processed as a negative control on 0.22 µm Sterivex filters.

Environmental and Spatial Factors

Environmental monitoring included HOBO data loggers recording dissolved oxygen, light, salinity, and temperature over the two-year deployment period. Water-column visibility (an inverse proxy for turbidity/nepheloid intensity) was estimated from ROV 4K video using parallel lasers (10 cm spacing) as scale. Eight experienced divers, blinded to site and depth, provided visibility estimates that were standardized within diver and ranked (1 = clearest to 13 = most turbid); site-level means were used as the turbidity metric. Satellite-derived oceanographic variables from Global Ocean Colour (Copernicus-GlobColour) database at a 4km resolution for the study region included chlorophyll-a, absorption coefficients, suspended matter, and surface primary productivity. Principal component analysis identified collinear variables, with depth, turbidity, and primary productivity retained as non-collinear predictors (**Fig. S1**).

DNA Extraction, Metabarcoding, and Sequencing

DNA from sessile and motile fractions was extracted with the Qiagen DNeasy PowerMax Soil Kit. Marine eukaryotic diversity was assessed by amplifying cytochrome oxidase subunit I (COI) and 18S V4 loci according to methods described in (Casey *et al.* 2021; Ransome *et al.* 2017). For niskin eDNA samples, DNA was extracted according to protocols detailed in (McCartin *et al.* 2024). Triplicate PCR reactions were performed per sample, pooled, verified, and sequenced on the Illumina MiSeq platform. Each ARMS contributed three metabarcoded fractions (sessile, 100 µm, 500 µm). The motile >2mm fraction was morphologically sorted, counted, and voucher tissues from both the sessile and motile fractions were barcoded by Sanger sequencing (COI Folmer region; Geller primers; (Geller *et al.* 2013)) and by shallow whole-genome "genome skimming." Phenol–chloroform extractions (Autogenprep 965) were used for vouchers; genome-skimming libraries were prepared using NEBNext Ultra II FS protocols

with modifications as in (Hoban *et al.* 2022). Sequences and metadata were deposited in GEOME (https://n2t.net/ark:/21547/EBk2) and NCBI. Reads were demultiplexed, QC-checked (FastQC), and trimmed (cutadapt). DADA2 was used for metabarcoding data filtering, error modeling, chimera removal, and ASV inference. Taxonomic classification used a custom hierarchical pipeline leveraging multiple reference databases and voucher specimens in a prioritized approach (NMNH voucher specimens > MetaZooGene marine references > NCBI). Post-assignment processing included backfilling missing taxonomy ranks using WoRMS (World Registry of Marine Species) API.

Plate Image Analysis

All plates were photographed and annotated in CoralNet(Beijbom 2015; Beijbom *et al.* 2015; Chen *et al.* 2021; Williams *et al.* 2019). We followed protocols from the Global ARMS Program site (https://naturalhistory.si.edu/research/global-arms-program/protocols). We trained on manually-scored images, then applied semi-automated classification with full manual verification. A standardized grid of 15 x 15 points was used for annotation, with both manual scoring and semi-automated classification followed by verification. CoralNet outputs were compared with metabarcoding at the phylum level.

Hydrodynamic Modeling

The Coastal and Regional Ocean Community model (CROCO) simulated ocean conditions at 1km resolution with 50 vertical layers. Three-dimensional hydrodynamic fields were saved every 30 minutes. Ichthyop v3.3.16 simulated particle advection with 40,000 particles released near sampling locations and followed for 20-40 days. Three dispersal scenarios were implemented: passive advection and two ontogenic vertical migration patterns (OVM-2 and OVM-10).

Statistical Analyses

Data Transformation

To mitigate dominance in metabarcoding data, we compared untransformed, Hellinger, and fourth-root transformations; fourth-root minimized NMDS stress and was adopted. NMDS used Bray-Curtis dissimilarity distances on rarefied ASV matrices (metabarcoding) or proportional/count data (CoralNet, 2 mm fauna) to visualize patterns across gradients and sites.

Alpha Diversity

Observed richness, Shannon, and Pielou's evenness were computed (vegan). For ARMS metabarcoding (COI, 18S), linear mixed-effects models tested size fraction, environmental gradients (depth, turbidity), and site, with ARMS ID as a random intercept (lmerTest). Rarefaction controlled for library size. For

eDNA (18S), general linear models tested environment and site; post-hoc tests were conservative given limited replication. For CoralNet and 2 mm fauna (coarser taxonomy, smaller n), we emphasized descriptive statistics and non-parametric correlations with depth and turbidity.

Beta Diversity

PERMANOVA (adonis; Bray–Curtis on fourth-root data) tested environmental (depth, turbidity), spatial (latitude, longitude), and site effects; dispersion was checked (PERMDISP). Conditional models partitioned variance into environment | geography (environmental filtering), geography | environment (dispersal limitation or unmeasured spatial processes), and site | all (local heterogeneity). dbRDA (capscale) and vector fitting (envfit) corroborated drivers. Distance-based tests (Mantel, partial Mantel, and MRM) related community dissimilarity to environmental and geographic distances (depth, turbidity, PP where applicable; least-cost seascape distances).

Taxon-Specific Responses

For metabarcoding, differential abundance across gradients used ANCOM-BC2 with FDR control; analyses were run on full, sessile-only, and motile-only subsets. For visual datasets, SIMPER identified contributors to between-group dissimilarities. Significant taxa were identified using Benjamini-Hochberg adjusted p-values ($q<0.05$).

Functional Analysis

To evaluate functional responses to turbidity, families in the 18S ARMS dataset were assigned to suspension-feeding and non-suspension categories (with sub-mechanistic classes for suspension feeders) based on literature (see **Table S1**). Group-level effect sizes (mean log-fold changes) were calculated for functional groups showing significant turbidity responses. Functional composition was compared between high and low turbidity sites, and functional diversity metrics were tested for correlation with environmental gradients.

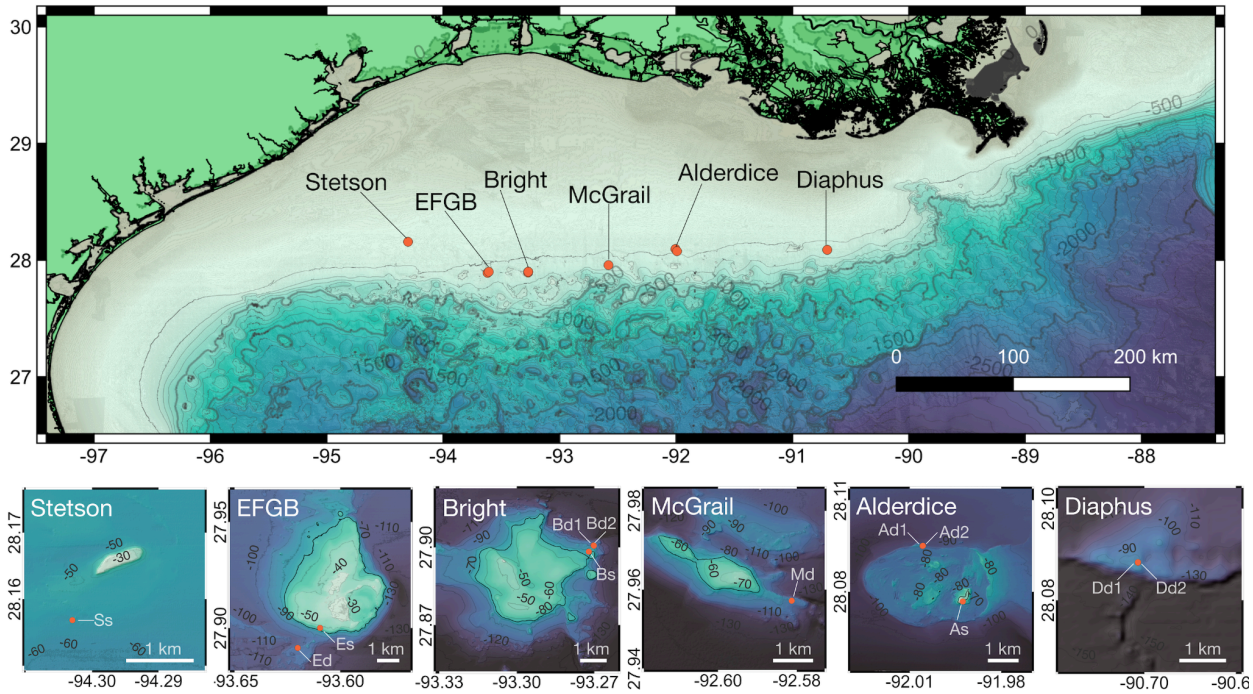

Figure 1. Sampling locations of ARMS units on the TX-LA shelf. (A) Bathymetric map of the six reef banks: Stetson, EFGB (East Flower Garden Bank), Bright, McGrail, Alderdice, and Diaphus. Contour lines represent depth in meters. (B) Detailed bathymetric maps of each site showing specific ARMS deployment locations, with colored markers indicating shallow and deep deployments. At each site, ARMS units were deployed at different depths, with some sites having multiple deep deployments (deep1, deep2). Site abbreviations follow the coding system: first letter of site name followed by deployment type (e.g., As = Alderdice shallow, Bd1 = Bright deep1). Scale bars represent 200 km for the overview map and 1 km for each detailed site map.

RESULTS

Dataset Overview and Quality Control

After quality filtering, rarefaction, and taxonomic classification three robust metabarcoding datasets were retained. We excluded COI-targeted eDNA samples from further analysis due to their significantly lower metazoan recovery rate, which would have limited our ability to assess eukaryotic community structure across sites. Rarefaction curves approached or reached asymptotes in all datasets (**Fig. S2**), indicating adequate sampling depth for community characterization across mesophotic banks of the TX-LA shelf. Visual datasets showed complementary biodiversity patterns, with 612 ARMS plate images annotated. We collected 1,858 tissue samples and barcoded one to three representatives of sessile and motile voucher morphospecies. Taxonomic analysis of barcoded macrofauna identified 8 phyla, 46 classes, 64 orders, 137 families, and 196 morphospecies.

Alpha Diversity Patterns

Diversity varied by fraction, method, and site. In COI-ARMS, size fraction had strong effects (Type II Wald χ^2: richness: $\chi^2 = 57.9$, $p < 0.001$; evenness: $\chi^2 = 74.6$, $p < 0.001$; Shannon: $\chi^2 = 40.7$, $p < 0.001$; Simpson: $\chi^2 = 34.9$, $p < 0.001$), with sessile samples exhibiting higher richness (276 ± 7.1 ASVs) but lower evenness (J' = 0.558 ± 0.009) than motile fractions (100 µm: 249 ± 5.4 ASVs, J' = 0.622 ± 0.009; 500 µm: 226 ± 5.8 ASVs, J' = 0.642 ± 0.009). Planned contrasts confirmed greater richness (+36.5 ± 5.5 ASVs, $p < 0.001$) in sessile vs. pooled motile fractions and lower evenness (-0.074 ± 0.009, $p < 0.001$). In 18S-ARMS, richness did not differ by size fraction (Type II Wald χ^2: $\chi^2 = 1.12$, $p = 0.57$) but evenness and Shannon diversity were higher in the 100 µm motile fraction (J' = 0.767 ± 0.022; H' = 6.19 ± 0.16, $p < 0.001$) than in sessile or 500 µm fractions (J' = 0.613-0.623, H' = 4.89-4.92,$p < 0.001$).

Fractions captured distinct components of the cryptobenthos. Only ~22% (COI) and ~16% (18S) of ASVs were shared among all three fractions; each fraction contributed substantial unique diversity, consistent with niche partitioning (COI, sessile: 34.2%, 100 µm: 34.3%, and 500 µm: 34.3%; 18S, 100 µm: 49.3%, sessile: 41.9%, and 500 µm: 31.5%. Site effects were pervasive. For COI-ARMS, all diversity metrics differed among sites (Type II Wald χ^2: $p < 0.001$). 18S-ARMS showed significant among-site differences for evenness and Shannon/Simpson (Type II Wald χ^2: $p < 0.02$; richness: $p = 0.38$), but not richness. For 18S-eDNA, 58.5% of ASVs occurred at a single site and mean inter-site Jaccard similarity was low (0.199, range: 0.095-0.361), indicating high spatial turnover. Morphological datasets showed lower variation overall: CoralNet yielded 8.42 ± 0.17 (mean ± SE) taxonomic groups per sample and barcoded motile macrofauna averaged 12 (IQR: 10-14) orders per ARMS unit.

Environmental effects were method-dependent. In COI-ARMS, depth consistently explained variation in richness, evenness, and diversity (marginal R^2 0.27-0.40; $\chi^2 = 5.3$-8.7; all $p \leq 0.022$). Turbidity affected evenness ($\chi^2 = 5.4$, $p = 0.020$) but not richness. In 18S-ARMS environmental relationships were weak (marginal $R^2 = 0.028$-0.285, all $p > 0.17$). CoralNet evenness declined with turbidity (Spearman: rho = -0.377, $p = 0.023$). Order-level richness of 2mm motile trended higher at turbid sites (+17.4%; Spearman: $\rho = 0.287$, $p = 0.089$). Together, these patterns indicate both environmental filtering and spatial structure, with COI communities showing the strongest environmental coupling.

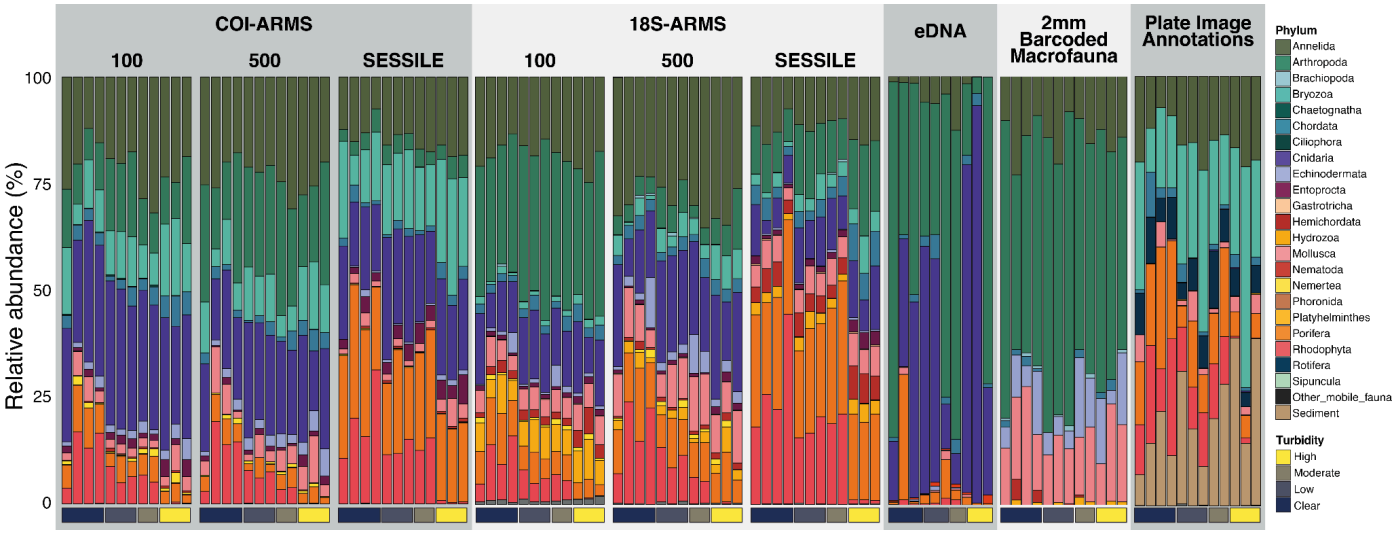

Figure 2. Relative abundance of taxonomically resolved marine metazoans across different biodiversity assessment methods. Abundance percentage (y-axis) of marine metazoan communities as detected by five different survey approaches: COI-ARMS, 18S-ARMS, 18S-eDNA, 2mm barcoded macrofauna, and ARMS plate image annotations. For both ARMS methods, data is further subdivided by size fraction (100 µm, 500 µm, and sessile). Each column represents all samples from each sampling site, arranged in order of increasing turbidity (left to right). Horizontal color bars at the bottom indicate relative turbidity levels from clear to high for visualization purposes, based on the standardized turbidity rank used in analysis.

Beta Diversity and Community Structure

Community composition varied with environment and space across all datasets (PERMANOVA: $p < 0.001$) (**Fig. 2**). Depth and turbidity were the dominant environmental axes. In ARMS assemblages, depth explained roughly 9–15% of variance ($p < 0.001$), with stronger vertical differentiation in sessile than motile fractions (PERMANOVA: $R^2 = 0.15$, $p < 0.001$). Turbidity also contributed consistently, particularly in CoralNet (PERMANOVA: $R^2 = 0.25$). Spatial predictors (latitude/longitude) explained ~14–25% of variance in ARMS datasets; latitude dominated in eDNA. Ordination reinforced these gradients (**Fig. 3**). In COI-ARMS, the first two axes captured ~21% of total compositional variance (rising to 36-42% in motile fractions and nearly 50% in sessile), aligned with depth and turbidity. 18S-ARMS PCoA showed similar alignment (first two axes ~20% of variance) (**Fig. S3**). Environmental fitting was strongest in eDNA, where depth alone explained 81% of variation in ordination space ($p < 0.001$). In CoralNet, turbidity was the leading correlate ($R^2 = 0.72$, $p < 0.001$), suggesting light attenuation and sediment load shape benthic recruitment. Local heterogeneity remained substantial. “Site” effects (beyond measured environment and space) explained 48% of variance in COI-ARMS, 38-68% in 18S-ARMS, 69% in eDNA, 71% in CoralNet, and 52% in barcoded macrofauna (PERMANOVA: all $p < 0.001$), consistent with unmeasured microhabitat variation or biotic interactions. Variance partitioning and dbRDA indicated that environmental predictors generally explained more variation than pure spatial terms (**Fig. S4**). In COI-ARMS, depth and turbidity together accounted for 18-28% of variance (each axis contributing ~10–15% and ~9–13%, respectively; all $p < 0.001$). Comparable values were observed in 18S-ARMS (17-29%). Adding spatial terms increased explained variance to 30-45%, reflecting the spatial autocorrelation of environmental gradients. After conditioning on environment, residual spatial structure (8-17%) persisted (all $p < 0.001$) indicating either dispersal limitation or unmeasured spatially structured factors. Pure environmental effects (independent of space) explained 12-16% of variance across ARMS datasets. Pure spatial effects explained 8-17% of variance, strongest in sessile assemblages (COI-ARMS: $R^2 = 0.174$; 18S-ARMS: $R^2 = 0.138$ for). Pure local effects were the largest in sessile communities (up to 23%, $p < 0.001$), highlighting fine-scale processes.

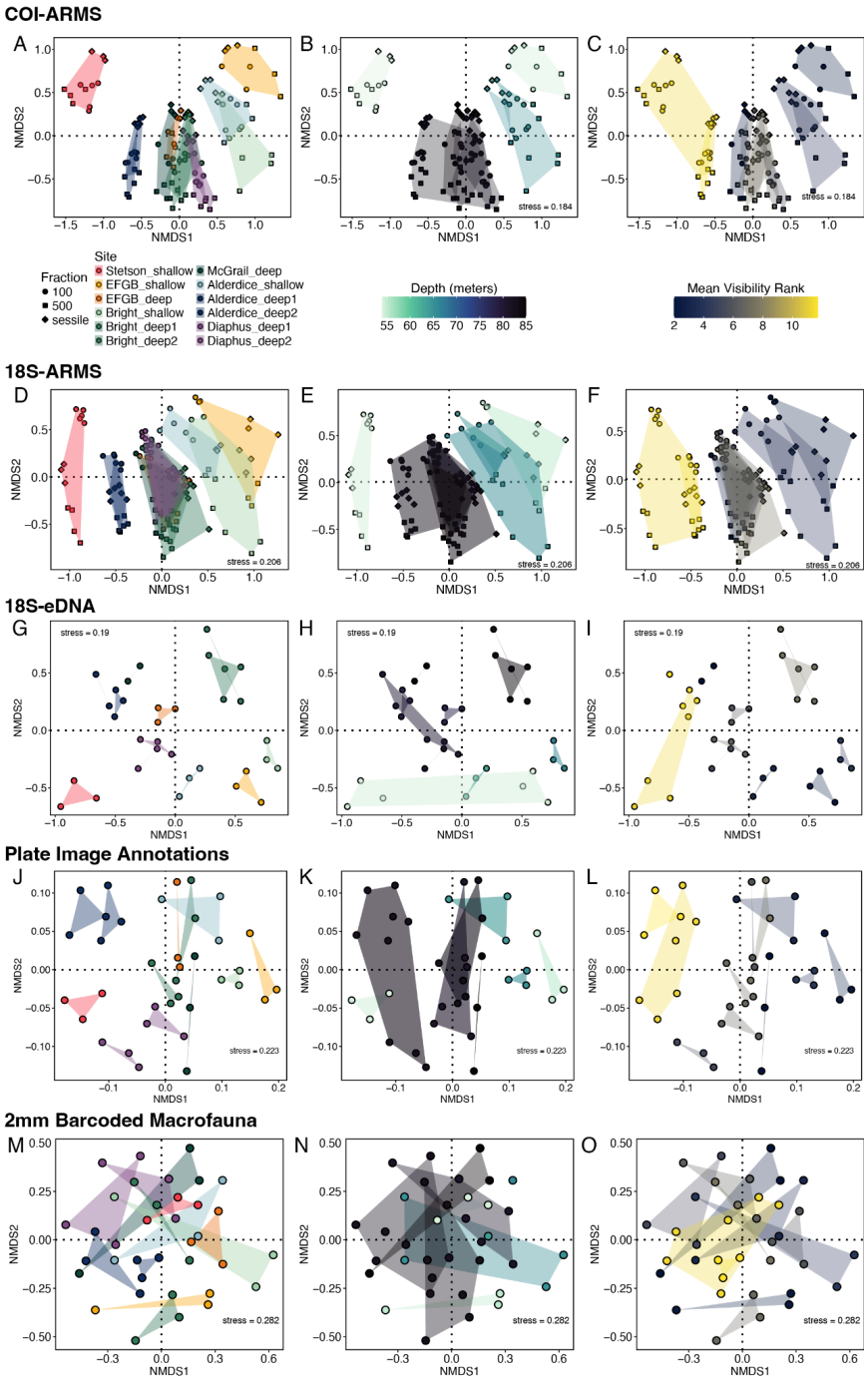

Figure 3. Non-metric multidimensional scaling (NMDS) ordination of marine community composition across different biodiversity assessment methods. NMDS plots based on Bray-Curtis dissimilarities of fourth-root transformed and rarefied ASV data. Rows represent different biodiversity assessment methods: COI-ARMS (A-C), 18S-ARMS (D-F), 18S-eDNA (G-I), Plate Image Annotations (J-L), and 2mm barcoded macrofauna (M-O). Columns show the same ordinations colored by different variables: sampling site (left column), depth in meters (middle column), and mean visibility rank as a proxy for turbidity (right column, higher values indicate lower visibility). Symbol shapes represent size fractions (100 µm, 500 µm, or sessile) as indicated in the legend. Colored polygons encompass samples from the same group. Stress values are displayed in the bottom right corner of applicable panels, indicating goodness-of-fit for the two-dimensional representation. NMDS axes are arbitrary units representing community dissimilarity, with points closer together indicating more similar community composition.

Hydrodynamic context

High-resolution simulations (1 km CROCO; 2014–2016 summers, chosen to capture significant Loop Current and mesoscale eddies variability and align with peak spawning periods) revealed strong spatiotemporal variability: a strong eastward jet south of 28°N (exceeding 0.8 m/s) opposed a weaker westward counterflow (<0.45 m/s) to the north, with frequent reversals and weakening events (zonal velocity SD > 0.25 m/s). Such variable flow conditions suggest that larvae released from the same location at different times could disperse in opposite directions depending on short-lived circulation dynamics. Lagrangian particle tracking (Ichthyop) showed bidirectional (east-west) connectivity among banks with marked interannual differences—fewest links in 2015 during a prolonged Loop Current intrusion; more in 2014 and 2016. Longer pelagic larval duration (40 vs. 20 d) increased connections by ~80–150% (**Fig. S5**). Ontogenetic vertical migration (short surface residence, OVM-2) yielded more successful connections than prolonged surface residence (OVM-10), which increased offshore advection; passive behavior produced intermediate connectivity between these scenarios. McGrail and Alderdice emerged as recurrent sources, with EFGB and Bright as major sinks. Edge sites (Stetson, Diaphus) contributed least to regional connectivity. Connection strengths were low (most <0.25%), indicating tenuous, time-sensitive exchanges. These dynamics are consistent with environmental filtering dominating regional turnover where dispersal opportunities exist but are variable.

Distance-based tests aligned with this interpretation (**Fig. S6a**). Environmental distance (depth + turbidity) strongly predicted community dissimilarity across metabarcoding datasets (Simple Mantel: COI-ARMS sessile $r = 0.824$, 18S-ARMS sessile $r = 0.826$, 18S-eDNA $r = 0.689$, all $p < 0.001$), even after controlling for spatial autocorrelation (Partial Mantel: COI-ARMS sessile $r = 0.803$, 18S-ARMS sessile $r = 0.807$, both $p < 0.001$). Geographic distance effects were 2-3 times weaker (Simple Mantel: $r = 0.076$-0.571) and often vanished after controlling for environment (Partial Mantel: 18S-ARMS motile $r = -0.032$, $p = 0.790$; 2mm fauna $r = 0.032$, $p = 0.217$) (**Fig S6b**). Multiple-regression-on-distance-matrices (MRM) analyses consistently favored environmental over geographic predictors, with coefficients 5-15 fold larger than geographic effects (MRM: 18S-ARMS sessile $\beta_env = 0.203$ vs $\beta_geo = 0.008$; CoralNet $\beta_env = 0.042$ vs $\beta_geo = 0.004$, all $p < 0.001$) (**Fig. S6c**). Sessile communities were highly predictable from environment (MRM: COI-ARMS $R^2 = 0.709$, 18S-ARMS $R^2 = 0.709$, CoralNet $R^2 = 0.295$, all $p < 0.001$), whereas motile and macrofaunal datasets fit more weakly (MRM: 18S-ARMS motile $R^2 = 0.478$, 2mm fauna $R^2 = 0.074$, both $p < 0.001$). eDNA showed more balanced influence between environmental facotrs (Simple Mantel: $r = 0.689$, $p < 0.001$) and spatial structure (Simple Mantel: $r = 0.571$, $p < 0.001$), with a residual spatial signal after controlling for environment (Partial Mantel: $r = 0.175$, $p < 0.001$). However, this difference may reflect temporal sampling scales: eDNA represents a community snapshot that captures recent dispersal events and temporary conditions, while ARMS communities developed over

two years, potentially revealing stronger, more stable environmental filtering patterns. Residual spatial structure (8-17% of variance) persisted beyond depth and turbidity across datasets, consistent with high, time-variable flow at deployment sites (velocity SD >0.25 m/s) and collinearity between environmental and spatial gradients (longitude-productivity r = 0.93; latitude-turbidity r = 0.54).

Environmental Filtering Effects

Abundance-based differential abundance analyses identified turbidity as the dominant environmental filter structuring communities across all datasets (metabarcoding and visual) and methods (ANCOMBC2 and SIMPER). Photoautotrophs declined consistently: Rhodophyta were lower in turbid sites across COI-ARMS (ANCOMBC2, log fold change [LFC] = -0.49, q = 4.1×10^{-15}), 18S-ARMS (ANCOMBC2, LFC = -0.56, q = 2.37×10^{-18}), CoralNet (2.6-fold higher in clear water, p_FDR = 0.003), and 18S-eDNA (Rhodymeniaceae LFC = -4.04, q = 3.0×10^{-12}), with family-level effects >50-fold for Rhodymeniaceae in eDNA. Heterotrophic Porifera declined with turbidity in COI-ARMS (LFC = -0.18, q = 0.016) and CoralNet (1.4-fold higher in clear water, p_FDR = 0.003).

In contrast, several heterotrophic groups increased with turbidity across datasets, including Bryozoa (ANCOMBC2, 18S-ARMS LFC = 0.17; CoralNet 1.15-fold higher in turbid water, p_FDR = 0.005). Entoprocta increased in 18S-ARMS LFC = 0.19), serpulid polychaetes (ANCOMBC2, LFC = 0.14; 1.14-fold higher, p_FDR = 0.003), and selected mobile taxa, including Platyhelminthes (COI-ARMS LFC = 0.32, q = 4.7×10^{-8}) and Chordata (ANCOMBC2, COI-ARMS LFC = 0.29, q = 2.9×10^{-5}). Depth effects were generally weaker and taxon-specific. Turbidity significantly affected 57% of phyla in COI-ARMS versus only 21% for depth, 115 families in 18S-ARMS versus 30 for depth, and 222 families in 18S-eDNA (55.5% turbidity, 14.1% depth). This dominance occurred despite turbidity and depth being uncorrelated (r = 0.14, p = 0.43), indicating independent environmental axes.

Depth effects were generally weaker and taxon-specific. In COI-ARMS, Cnidaria increased with depth (ANCOMBC2, LFC = 0.051, q = 7.1×10^{-6}) while Mollusca decreased (ANCOMBC2, LFC = -0.070, q = 2.5×10^{-4}). In 18S-eDNA, sponge families generally decreased with depth (ANCOMBC2, Suberitidae LFC = -0.55, q = 1.6×10^{-6}; Agelasidae LFC = -0.51, q = 2.2×10^{-5}; Spirastrellidae LFC = -0.38, q = 3.6×10^{-4}), while polychaete family Nephtyidae increased (ANCOMBC2, LFC = 0.35, q = 4.0×10^{-5}). Rhodymeniaceae exhibited a positive depth association in eDNA (ANCOMBC2, LFC = 0.66, q = 3.7×10^{-6}), potentially indicating deep-adapted lineages or accumulation of drift algae in deeper waters. CoralNet depth patterns were minimal after FDR correction, with only three phyla showing significant associations.

Site identity exerted strong taxon-level effects (global tests, q < 0.05 for 93% of phyla in ARMS), often exceeding single-gradient signals, consistent with local habitat variation and fine-scale processes. The magnitude of site effects (test statistics W = 4.6-69.8 in COI-ARMS; W = 11.03-28.96 in 18S-ARMS) exceeded environmental gradient effects. Size fraction also differed: in COI-ARMS most phyla (86%) varied among sessile, 100 µm, and 500 µm fractions, with the strongest effects in Porifera (W = 151.4), Arthropoda (W = 92.6), and Echinodermata (W = 58.5). In 18S-ARMS, 94% of phyla and

89% of families showed fraction effects, reflecting ecological segregation by size class. Motile and sessile fractions shared the direction of environmental responses but differed in site specificity (93% vs 77% of phyla varied by site in COI-ARMS), suggesting greater microhabitat coupling in sessile assemblages.

Primary productivity structured benthic and pelagic eDNA communities through subtle but widespread effects, with 69 families (30% of total effects) responding to the oligotrophic western to eutrophic eastern Gulf gradient (ANCOMBC2, median LFC = 0.004, all $q < 0.05$). Rhodymeniaceae declined with productivity (ANCOMBC2, LFC = -0.017, $q = 8.8\times10^{-10}$), while bioeroding Clionaidae (Porifera) (ANCOMBC2, LFC = 0.032, $q = 3.4\times10^{-8}$) and planktonic Salpidae (Chordata) (ANCOMBC2, LFC = 0.0028, $q = 7.6\times10^{-6}$) increased. Among molluscs, Mytilidae (ANCOMBC2, LFC = -0.0042, $q = 1.4\times10^{-6}$) and Calyptraeidae (ANCOMBC2, LFC = -0.0082, $q = 9.0\times10^{-6}$) declined with productivity. Fifty families responded to multiple gradients simultaneously, with 15 families responding to all three predictors (depth, turbidity, productivity), indicating complex niche structuring beyond single-axis environmental filtering. Barcoded macrofauna exhibited minimal taxon-specific environmental associations compared to sessile communities. Only one order (Valvatida, Echinodermata) showed significant turbidity association after FDR correction (5.1-fold higher in turbid water, p_FDR = 0.04), despite strong community-level environmental structure in ordination analyses. This pattern contrasted fundamentally with sessile CoralNet communities, which exhibited seven phyla with significant taxon-environment associations (p_FDR < 0.05). The disparity suggests mobile organisms can behaviorally select microhabitats or avoid unfavorable conditions, decoupling individual taxon distributions from environmental gradients, while sessile organisms remain constrained by local abiotic conditions.

Richness-based functional analyses supported two mechanistic pathways of turbidity filtering (97 families showed significant turbidity responses)(**Fig. 4, Fig. S7**). First, light limitation reduced photoautotrophs, particularly coralline algae families (PHOT; n=12, mean LFC = 0.04 ± 0.12 SE). Second, sediment load disfavored fine-pore microfilterers (sponges) while favoring particle-sorting suspension feeders with rejection mechanisms. Active dead-end sieves (ADS; n=11 families, e.g., certain bivalves/barnacles/polychaetes) increased with turbidity (mean LFC = + 0.09 ± 0.03 SE, 85% of families increasing); fine dead-end microfilterers (FDM; n=5, e.g., sponges) decreased. Parasites (n=9, mean LFC = +0.19 ± 0.17), grazers (n=5, mean LFC = +0.15 ± 0.10 SE), and predators (n=22, mean LFC = +0.15 ± 0.12 SE) tended to increase, and deposit feeders were stable (n=16, mean LFC = -0.053 ± 0.066 SE), though within-group heterogeneity was high ($P > 0.18$). Across sites, low turbidity coincided with higher photoautotroph (3.5x) and FDM-sponge (2.1x) representation, whereas high turbidity shifted communities toward active suspension feeders (ADS; 1.6x higher than in low turbidity).

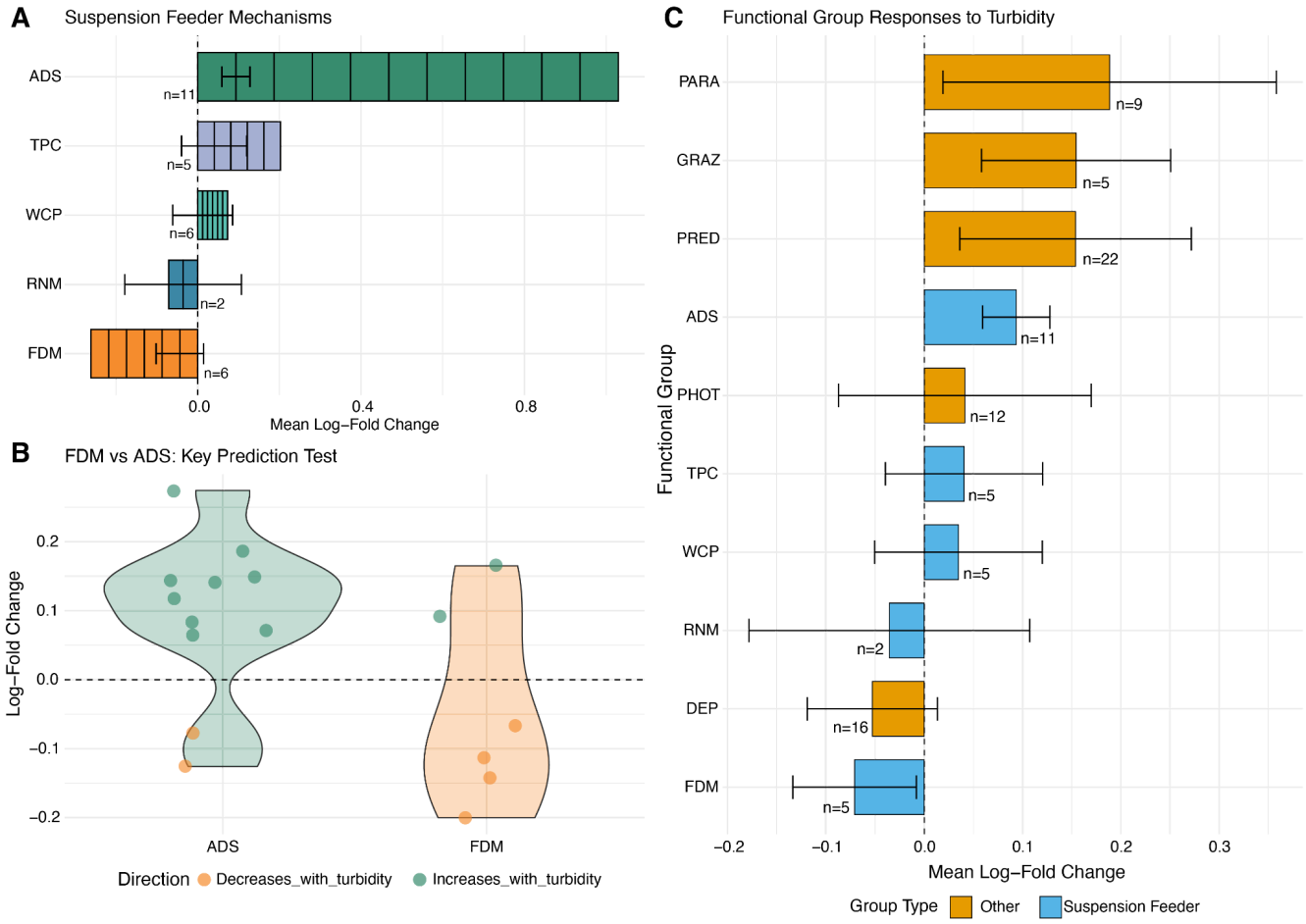

Figure 4. Functional feeding group responses of 18S-ARMS rDNA taxa to turbidity gradients. A) Mean log-fold change (LFC) by suspension feeding mechanism, showing ADS increasing and FDM decreasing with turbidity. B) Individual family responses for FDM vs ADS. Colors indicate response direction (green = increases, orange = decreases) C) Mean LFC in relative abundance across turbidity gradient for functional groups consisting of greater than > 3 significant families (ANCOM-BC2, $q < 0.05$, all samples). Error bars represent ± 1 SE. Suspension feeders (blue) show divergent responses by mechanism: ADS = Active Dead-End Sieves, FDM = Fine Dead-End Microfilterers, Other functional groups (orange) abbreviations: DEP = deposit feeders, PHOT = photoautotrophs, WCP = weak ciliary pumpers, TPC = truly passive collectors, RNM = renewable mucus nets, PRED = predators, GRAZ = grazers, PARA = parasites).

DISCUSSION

This study provides the first integrated view of mesophotic cryptobenthic communities across the Texas–Louisiana (TX–LA) continental shelf, revealing how environmental filtering, dispersal processes, and local heterogeneity jointly structure biodiversity. By combining standardized colonization substrates (ARMS), metabarcoding, eDNA, image-based surveys, and hydrodynamic modeling, we demonstrate that community assembly in these mesophotic systems is governed primarily by environmental filtering, especially turbidity, while spatial and dispersal processes exert secondary, scale-dependent influences. These results advance understanding of metacommunity dynamics in the mesophotic realm and highlight the ecological distinctiveness of these deeper reef systems within the broader Gulf mosaic.

Environmental filtering as the primary driver of metacommunity structure

Our findings provide strong support for the environmental filtering hypothesis, indicating that species sorting is the primary metacommunity process structuring mesophotic reef assemblages across the northwestern TX-LA continental shelf. Across datasets and analytical frameworks, turbidity associated with the benthic nepheloid layer emerged as the most consistent and powerful environmental driver. It structured community composition, functional composition, and taxon-specific abundances, surpassing the influence of depth and geography. Turbidity and its correlates, light attenuation, sedimentation, and reduced primary productivity, impose strong physiological and functional constraints on sessile reef organisms (Anthony & Fabricius 2000; Erftemeijer *et al.* 2012). In our study, photoautotrophic and fine-pore suspension-feeding taxa abundance declined steeply with increasing turbidity while particle-sorting and mucus-net feeders increased, reflecting functional replacement rather than loss of biodiversity. These shifts parallel patterns documented on turbid shallow reefs worldwide (e.g., (Morgan *et al.* 2020) but extend them into the mesophotic zone, where suspended particulates and the benthic nepheloid layer act as persistent filters shaping species turnover. Our findings enhance the understanding of zonation patterns (Gittings *et al.* 1992; Rezak *et al.* 1990) by quantifying how they manifest in metacommunity structure. Near-bottom dynamics create strong environmental filtering effects that determine community composition, with sufficient physical connectivity enabling species to track suitable environmental conditions rather than being constrained by dispersal capabilities.

Depth also contributed to environmental sorting but with weaker and more taxon-specific effects. Depth-associated gradients in light, temperature, and hydrostatic pressure influenced certain groups, particularly rhodophytes, cnidarians, mollusks, and entoprocts but did not produce the strong, community-wide stratification observed for turbidity. This asymmetry underscores that on the shelf, turbidity is a more pervasive and heterogeneous driver than depth *per se,* partially independent of broad geographic gradients, and exserting localized effects even at comparable depths., and exerting localized

effects even at comparable depths. Together, these findings indicate that environmental filtering along independent turbidity and depth axes drives compositional differentiation across mesophotic banks, consistent with predictions of species-sorting paradigms of metacommunity theory.

Spatial structure and dispersal processes

Although environmental filtering dominated, spatial effects were significant across all datasets. Variance partitioning revealed pure spatial components (8-17% of variance) and residual spatial structure beyond measured environmental gradients, suggesting a role for limited dispersal among banks, unmeasured spatially structured habitat differences, or lingering effects of past colonization and disturbance.

The particle-tracking experiments demonstrated that short-lived buoyant phases and rapid return to near-bottom depths maximize cross-bank exchange, whereas prolonged surface residence leads to advection losses. This pattern mirrors empirical observations in benthic invertebrates with short-lived larvae and supports the notion that dispersal limitation in these systems operates primarily through behavioral or ontogenetic constraints rather than absolute distance (Cowen & Sponaugle 2009; Lett *et al.* 2015). The weak relationship between geographic and community dissimilarity further supports a model of high but variable connectivity coupled with strong local environmental filtering, a combination characteristic of weakly coupled metacommunities (Holyoak *et al.* 2005; Leibold *et al.* 2004).

Functional and taxonomic turnover across environmental gradients

Environmental filtering manifested not only as compositional shifts but also as functional reorganization. Turbidity gradients reshaped the balance among feeding guilds, reducing the relative abundance of photoautotrophs and microfiltering sponges while favoring active suspension feeders with particle rejection mechanisms. These patterns reflect differential sediment tolerance and suggest that sediment loading selects for taxa capable of maintaining feeding efficiency under reduced flow or elevated particulate loads (Riisgård & Larsen 2010). Functional composition thus provides a mechanistic link between community turnover and ecosystem function, implying that changes in turbidity alter benthic productivity, nutrient recycling, and habitat complexity.

The magnitude of functional turnover was greatest in sessile assemblages and smallest in transient or motile taxa. Sessile organisms are directly exposed to sediment stress and cannot behaviorally avoid unsuitable conditions, whereas mobile fauna can exploit microhabitats or migrate (Beauchard *et al.* 2022; Diaz & Rosenberg 1995; Norkko *et al.* 2010),explaining the weaker environmental correlations and lower model fits observed for motile and macrofaunal datasets. Similar environmentally driven structuring in sessile ARMS cryptobiomes has been documented across deployments worldwide (Pearman *et al.* 2018;

Villalobos *et al.* 2024). Collectively, the results indicate that environmental filtering acts most strongly on attached taxa, which anchor community structure and provide the substrate for subsequent colonization by motile species.

Local heterogeneity and fine-scale assembly processes

Local effects accounted for the largest share of unexplained variance across all datasets, especially in sessile fractions. This residual variation likely reflects unmeasured microhabitat attributes such as substrate texture, microtopography, hydrodynamic exposure, and biological interactions that modulate colonization and survival. Within the ARMS units themselves, plate position and light exposure can generate micro-gradients comparable to those on natural reef surfaces (Leray & Knowlton 2015). Such local-scale processes are integral to metacommunity dynamics. Even under strong regional filters, local heterogeneity sustains diversity by promoting coexistence through niche partitioning and stochastic recruitment (Chase & Myers 2011). The contrast between molecular and morphological datasets also emphasizes the importance of taxonomic resolution and detection sensitivity in interpreting assembly processes. Metabarcoding revealed substantial cryptic turnover and high niche partitioning among fractions that were not evident from visual data alone, reinforcing the value of molecular tools for detecting biodiversity patterns in structurally complex environments.

Regional context and connectivity within the Flower Garden Banks system

The mesophotic banks of the Flower Gardens region form a distinctive ecological network linking shallow and deep benthic systems. Prior genetic and larval studies have shown that the populations of several megafaunal species (e.g., *Montastraea cavernosa*, *Lutjanus campechanus*) are well connected among banks (Studivan & Voss, 2018; Zhou et al., 2024), yet our results suggest that smaller, less mobile taxa experience stronger environmental filtering and habitat patch-specific differentiation. The weak geographic signals in our data, despite complex currents, imply that dispersal is sufficient to homogenize regional species pools, but local environmental and functional filters ultimately determine establishment success. This pattern is emblematic of metacommunity “mass-effect” dynamics, where regional dispersal maintains potential connectivity without eliminating local environmental control.

The hydrodynamic model results provide important context for conservation. Bidirectional, temporally variable connectivity suggests that larval exchange among banks is episodic and asymmetric, making certain banks, particularly McGrail and Alderdice, critical sources, while others (e.g., East and West Flower Garden Banks) function as persistent sinks. These dynamics underscore the value of spatially distributed protection within the Flower Garden Banks National Marine Sanctuary, as loss or degradation of key source banks could disrupt recruitment across the network.

Implications for biodiversity monitoring and management

The methodological integration applied here (standardized ARMS sampling, metabarcoding, eDNA, and hydrodynamic modeling) offers a scalable framework for long-term biodiversity monitoring in mesophotic ecosystems. The strong correspondence between environmental gradients and community structure indicates that turbidity and depth can serve as practical indicators for tracking ecological change. The ARMS-metabarcoding approach effectively captured both sessile and motile cryptofauna fractions, revealing ecological patterns that complement and extend traditional imagery and specimen-based surveys. Importantly, these standardized approaches provide a reproducible basis for time-series comparisons, facilitating detection of community shifts driven by climate, sedimentation, or management interventions.

From a management perspective, the dominance of water turbidity as an environmental filter highlights the sensitivity of mesophotic assemblages to sediment dynamics. Turbidity over the shelf is influenced by riverine inputs, resuspension, and benthic trawling, all processes expected to change under anthropogenic pressure and environmental change (Gil-Agudelo *et al.* 2020)(Rocha *et al.* 2018; Turner *et al.* 2017)(Gil-Agudelo *et al.* 2020). Our results offer a framework for conservation planning in other continental margin mesophotic systems experiencing similar oceanographic conditions. Comparable nepheloid-influenced assemblages exist along continental shelves worldwide, including off northwestern Australia (Collins *et al.* 2015), the Bay of Biscay (van den Beld *et al.* 2017), the Namibian margin (Tamborrino *et al.* 2022), and the northeast Atlantic margin (Morrissey *et al.* 2023; Wilson *et al.* 2015). Protecting water quality and minimizing sediment disturbance are therefore essential for maintaining the ecological integrity of these ecosystems. Moreover, functional turnover toward sediment-tolerant assemblages reflects a shift in community composition rather than reduced richness, with substantial declines in sessile habitat-forming taxa such as coraline aglae and sponges potentially affecting habitat complexity and associated ecosystem services.

Beyond our study region, our findings emphasize that effective management of MCEs must account for the complex interplay between regional oceanographic processes, local environmental conditions, and community assembly mechanisms to ensure the persistence of these unique and underexplored ecosystems. By demonstrating that cryptobenthic assemblages track fine-scale environmental gradients despite potential connectivity, this study refines our understanding of biodiversity organization in mesophotic reef systems. It extends metacommunity theory into an underexplored depth zone and establishes an empirical foundation for standardized, multiscale monitoring across the Flower Garden Banks network and comparable mesophotic habitats worldwide.

Author Contributions

S.H. and C.P.M conceptualized and designed the study, and acquired funding. L.W. adapted ARMS and recovery crate for deep-sea application. N.C.P, L.J.M, S.M.T., S.A.V., C.P.M., and S.H. acquired the field samples. N.C.P. and L.J.M. performed laboratory work and data analysis. S.M.T. and K.D. sequenced voucher specimens. S.M. and J.L. processed and annotated plate images. L.L. and A.B. conceived and conducted model simulations, L.L. performed the model simulations and analysis. N.C.P. drafted the manuscript. All authors contributed to interpretation of the data and writing.

Acknowledgments

This research was funded by NOAA's National Centers for Coastal Ocean Science, Competitive Research Program and Office of Ocean Exploration and Research under award NA18NOS4780166 to Lehigh University. S.H. is supported by the National Academies of Sciences, Engineering, and Medicine Gulf Research Program Early-Career Fellowship under award 2000013668, and N.P. is supported by a National Science Foundation Graduate Research Fellowship. Voucher sequencing was conducted in and with the support of the Laboratories of Analytical Biology (https://ror.org/05b8c0r92) facilities of the Smithsonian National Museum of Natural History. The authors thank Dr. Corinna Breusing for voucher specimen genome skimming library preparation and data processing. We thank the Underwater Acoustics Society and Dr. Kirstin Meyer-Kaiser for assistance in estimating visibility for turbidity estimates. We are grateful to Dr. Daniel Fornari for building the benthic lander used to recover ARMS units, and to Dr. Jill McDermott and Katie Foley for their assistance in ARMS deployment. We appreciate the contributions of Abby Uheling, Maria Granquist, Emma Sasso, Penny Demetriades, and Luis Caceres for their assistance in ARMS recovery and processing. We extend our thanks to the Captain and crew of R/V *Manta* and R/V *Point-Sur*, as well as Oceaneering Inc ROV technicians. Special thanks to the Flower Garden Banks National Marine Sanctuary staff (G.P. Schmall, Emma Hickerson, Marissa Nuttall, and Michelle Johnston) for their invaluable support of this study. We also thank Weihua Wang from the Genomics Research Core at the University of Illinois Chicago, and Dr. Stefan Green, Cecilia Chau, and Ashley Wu from the Genomics and Microbiome Core Facility at Rush Medical University for library preparation and sequencing.

REFERENCES

Anderson, M.J. (2001). A new method for non‐parametric multivariate analysis of variance. *Austral Ecol.*, 26, 32–46.

Anderson, M.J., Ellingsen, K.E. & McArdle, B.H. (2006). Multivariate dispersion as a measure of beta diversity. *Ecol. Lett.*, 9, 683–693.

Andrews, S. & Others. (2010). FastQC: a quality control tool for high throughput sequence data.

Anthony, K.R. & Fabricius, K.E. (2000). Shifting roles of heterotrophy and autotrophy in coral energetics under varying turbidity. *J. Exp. Mar. Bio. Ecol.*, 252, 221–253.

Aronson, R.B., Precht, W.F., Murdoch, T.J.T. & Robbart, M.L. (2005). Long-Term Persistence of Coral Assemblages on the Flower Garden Banks, Northwestern Gulf of Mexico: Implications for Science and Management. *Gulf Mex. Sci.*, 23, 6.

Auclair, F., Benshila, R., Bordois, L., Boutet, M. & Brémond, M. (2019). Coastal and Regional Ocean COmmunity model (1.1), Zenodo [code].

Bartoń, K. (2022). MuMIn: multi-model inference. *R package version 1.46. 0.*

BBMap. (2022). *SourceForge*. Available at: https://sourceforge.net/projects/bbmap. Last accessed 2 November 2025.

Beauchard, O., Mestdagh, S., Koop, L., Ysebaert, T. & Herman, P.M.J. (2022). Benthic synecology in a soft sediment shelf: habitat contrasts and assembly rules of life strategies. *Mar. Ecol. Prog. Ser.*, 682, 31–50.

Beijbom, O. (2015). Automated Annotation of Coral Reef Survey Images. UC San Diego.

Beijbom, O., Edmunds, P.J., Roelfsema, C., Smith, J., Kline, D.I., Neal, B.P., *et al.* (2015). Towards automated annotation of benthic survey images: Variability of human experts and operational modes of automation. *PLoS One*, 10, e0130312.

van den Beld, I.M.J., Bourillet, J.-F., Arnaud-Haond, S., de Chambure, L., Davies, J.S., Guillaumont, B., *et al.* (2017). Cold-Water coral habitats in submarine canyons of the bay of Biscay. *Front. Mar. Sci.*, 4.

Bolger, A.M., Lohse, M. & Usadel, B. (2014). Trimmomatic: a flexible trimmer for Illumina sequence data. *Bioinformatics*, 30, 2114–2120.

Bongaerts, P., Ridgway, T., Sampayo, E.M. & Hoegh-Guldberg, O. (2010). Assessing the “deep reef refugia” hypothesis: focus on Caribbean reefs. *Coral Reefs*, 29, 309–327.

Brandl, S.J., Goatley, C.H.R., Bellwood, D.R. & Tornabene, L. (2018). The hidden half: ecology and evolution of cryptobenthic fishes on coral reefs: Cryptobenthic reef fishes. *Biol. Rev. Camb. Philos. Soc.*, 93, 1846–1873.

Callahan, B.J., McMurdie, P.J., Rosen, M.J., Han, A.W., Johnson, A.J. & Holmes, S.P. (2015). DADA2: High resolution sample inference from amplicon data. *bioRxiv*.

Casey, J.M., Ransome, E. & Collins, A.G. (2021). DNA metabarcoding marker choice skews perception of marine eukaryotic biodiversity. *Environmentalist*.

Chase, J.M. & Myers, J.A. (2011). Disentangling the importance of ecological niches from stochastic processes across scales. *Philos. Trans. R. Soc. Lond. B Biol. Sci.*, 366, 2351–2363.

Chen, Q., Beijbom, O., Chan, S., Bouwmeester, J. & Kriegman, D. (2021). A new deep learning engine for CoralNet. In: *2021 IEEE/CVF International Conference on Computer Vision Workshops (ICCVW)*. Presented at the 2021 IEEE/CVF International Conference on Computer Vision Workshops (ICCVW), IEEE, pp. 3693–3702.

Chen, S., Zhou, Y., Chen, Y. & Gu, J. (2018). fastp: an ultra-fast all-in-one FASTQ preprocessor. *Bioinformatics*, 34, i884–i890.

Clarke, K.R. (1993). Non‐parametric multivariate analyses of changes in community structure. *Aust. J. Ecol.*, 18, 117–143.

Clarke, K.R. & Gorley, R.N. (2015). Getting started with PRIMER v7. *PRIMER-e: plymouth, plymouth marine laboratory*.

Collins, L.B., O'Leary, M., Stevens, A., Bufarale, G., Kordi, M. & Solihuddin, T. (2015). Geomorphic patterns, internal architecture and reef growth in a macrotidal, high-turbidity setting of coral reefs from the Kimberley bioregion. *Aust. J. Marit. Ocean Aff.*, 7, 12–22.

Cordes, E.E., Gasbarro, R., Quattrini, A.M., Stabbins, A., Georgian, S.E., Carney, R.S., *et al.* (2025). Do chemosynthetic and coral communities defy deep‐sea ecological paradigms? *Glob. Ecol. Biogeogr.*, 34, e70039.

Cottenie, K. (2005). Integrating environmental and spatial processes in ecological community dynamics. *Ecol. Lett.*, 8, 1175–1182.

Cowen, R.K. (2002). Oceanographic influences on larval dispersal and retention and their consequences for population connectivity In Sale PF, editor.

Cowen, R.K. & Sponaugle, S. (2009). Larval dispersal and marine population connectivity. *Ann. Rev. Mar. Sci.*, 1, 443–466.

Cristescu, M.E. (2014). From barcoding single individuals to metabarcoding biological communities: towards an integrative approach to the study of global biodiversity. *Trends Ecol. Evol.*, 29, 566–571.

Cummings, J.A. (2005). Operational multivariate ocean data assimilation. *Q. J. R. Meteorol. Soc.*, 131, 3583–3604.

Cummings, J.A. & Smedstad, O.M. (2013). Variational Data Assimilation for the Global Ocean. In: *Data Assimilation for Atmospheric, Oceanic and Hydrologic Applications (Vol. II)*. Springer Berlin

Heidelberg, Berlin, Heidelberg, pp. 303–343.

Dennis, G.D. & Bright, T.J. (1988). Reef fish assemblages on hard banks in the northwestern Gulf of Mexico. *Bull. Mar. Sci.*

Diaz, R.J. & Rosenberg, R. (1995). Marine Benthic Hypoxia: a review of its ecological effects and the behavioural responses of benthic macrofauna. *Oceanogr. Mar. Biol. Annu. Rev.*, 33, 245–303.

Egbert, G.D. & Erofeeva, S.Y. (2002). Efficient inverse modeling of barotropic ocean tides. *J. Atmos. Ocean. Technol.*, 19, 183–204.

Enochs, I.C. (2012). Motile cryptofauna associated with live and dead coral substrates: implications for coral mortality and framework erosion. *Mar. Biol.*, 159, 709–722.

Erftemeijer, P.L.A., Riegl, B., Hoeksema, B.W. & Todd, P.A. (2012). Environmental impacts of dredging and other sediment disturbances on corals: a review. *Mar. Pollut. Bull.*, 64, 1737–1765.

Ewels, P., Magnusson, M., Lundin, S. & Käller, M. (2016). MultiQC: summarize analysis results for multiple tools and samples in a single report. *Bioinformatics*, 32, 3047–3048.

Eyal, G., Laverick, J.H., Bongaerts, P., Levy, O. & Pandolfi, J.M. (2021). Mesophotic coral ecosystems of the Great Barrier Reef are understudied and underexplored. *Front. Mar. Sci.*, 8, 622856.

Fenner, D. & Banks, K. (2004). Orange Cup Coral Tubastraea coccinea invades Florida and the Flower Garden Banks, Northwestern Gulf of Mexico. *Coral Reefs*.

Fleming, B.F.M., Beaulieu, S.E., Mills, S.W., Gaggiotti, O.E. & Mullineaux, L.S. (2022). Ecological connectivity in Pacific deep-sea hydrothermal vent metacommunities. *Mar. Ecol. Prog. Ser.*, MFC.

Fox, J. & Weisberg, S. (2018). *An R companion to applied regression*. 3rd edn. SAGE Publications, Thousand Oaks, CA.

Frattini, B., Bruggemann, H., Goberville, E., Couëdel, M., Bruggemann, F. & Guillaume, M.M.M. (2025). Deterministic and stochastic processes drive sessile cryptobenthic community composition on coral reefs at different spatial scales. *Mar. Ecol. Prog. Ser.*, 761, 21–34.

Frøslev, T.G., Kjøller, R., Bruun, H.H., Ejrnæs, R., Brunbjerg, A.K., Pietroni, C., *et al.* (2017). Algorithm for post-clustering curation of DNA amplicon data yields reliable biodiversity estimates. *Nat. Commun.*, 8, 1188.

Galaska, M.P., Liu, G., West, D. & Erickson, K. (2021). Seascape genomics reveals metapopulation connectivity network of Paramuricea biscaya in the northern Gulf of Mexico. *Frontiers in Marine*.

Garavelli, L., Studivan, M.S., Voss, J.D., Kuba, A., Figueiredo, J. & Chérubin, L.M. (2018). Assessment of Mesophotic Coral Ecosystem Connectivity for Proposed Expansion of a Marine Sanctuary in the Northwest Gulf of Mexico: Larval Dynamics. *Frontiers in Marine Science*, 5.

Gardner, J.V., Mayer, L.A., Hughes Clark, J.E. & Kleiner, A. (1998). High-Resolution Multibeam Bathymetry of East and West Flower Gardens and Stetson Banks, Gulf of Mexico. *Gulf Mex. Sci.*,

16, 3.

Geller, J., Meyer, C. & Parker, M. (2013). Redesign of PCR primers for mitochondrial cytochrome c oxidase subunit I for marine invertebrates and application in all‐taxa biotic surveys. *Mol. Ecol.*

Gil-Agudelo, D.L., Cintra-Buenrostro, C.E., Brenner, J., González-Díaz, P., Kiene, W., Lustic, C., *et al.* (2020). Coral Reefs in the Gulf of Mexico Large Marine Ecosystem: Conservation Status, Challenges, and Opportunities. *Frontiers in Marine Science*, 6.

Ginsburg, R.N. (1983). Geological and biological roles of cavities in coral reefs.

Gittings, S.R., Boland, G.S., Deslarzes, K.J.P., Hagman, D.K. & Holland, B.S. (1992). Long-term monitoring at the East and West Flower Garden Banks. *US Dept. of the Interior, Minerals Management Service, Gulf of Mexico OCS Region, New Orleans, LA. OCS Study MMS*, 92–0006.

Hajibabaei, M., Spall, J.L., Shokralla, S. & van Konynenburg, S. (2012). Assessing biodiversity of a freshwater benthic macroinvertebrate community through non-destructive environmental barcoding of DNA from preservative ethanol. *BMC Ecol.*, 12, 28.

Heino, J., Melo, A.S., Siqueira, T., Soininen, J., Valanko, S. & Bini, L.M. (2015). Metacommunity organisation, spatial extent and dispersal in aquatic systems: patterns, processes and prospects. *Freshw. Biol.*, 60, 845–869.

Hickerson, E.L., Schmahl, G.P., Robbart, M., Precht, W.F. & Caldow, C. (2023). *The state of coral reef ecosystems of the flower garden banks, stetson bank, and other banks in the northwestern gulf of Mexico*. Available at: http://www.warcosts.net/wp-content/uploads/us-navy/317P_5_2008_NOAA_The_State_of_Coral_Reef_Ecosystems_of_the_U.S._and_Pacific_Freely_Associated_States_Report_Northwestern_Gulf_of_Mexico.pdf. Last accessed 6 October 2023.

Hoban, M.L., Whitney, J., Collins, A.G., Meyer, C., Murphy, K.R., Reft, A.J., *et al.* (2022). Skimming for barcodes: rapid production of mitochondrial genome and nuclear ribosomal repeat reference markers through shallow shotgun sequencing. *PeerJ*, 10, e13790.

Holstein, D.M., Smith, T.B., Gyory, J. & Paris, C.B. (2015). Fertile fathoms: Deep reproductive refugia for threatened shallow corals. *Sci. Rep.*, 5, 12407.

Holyoak, M., Leibold, M.A. & Holt, R.D. (2005). *Metacommunities: Spatial Dynamics and Ecological Communities*. University of Chicago Press.

Ip, Y.C.A., Chang, J.J.M., Oh, R.M. & Quek, Z.B.R. (2023). … ARMS shall find: DNA (meta) barcoding of Autonomous Reef Monitoring Structures across the tree of life uncovers hidden cryptobiome of tropical urban coral reefs. *Molecular*.

Johnstone, J.W., Jenkins, W.G., Jankiewicz, M., Quigley, J.M., Frometa, J., Salgado, E., *et al.* (2025). Spawning and larval development of the mesophotic octocoral Swiftia exserta in aquaria. *Mar. Biol.*,

172, 1–17.

Kuznetsova, A., Brockhoff, P.B. & Christensen, R.H.B. (2017). LmerTest package: Tests in linear mixed effects models. *J. Stat. Softw.*, 82, 1–26.

Langmead, B. & Salzberg, S.L. (2012). Fast gapped-read alignment with Bowtie 2. *Nat. Methods*, 9, 357–359.

Legendre, P., Borcard, D. & Peres-Neto, P.R. (2005). Analyzing beta diversity: Partitioning the spatial variation of community composition data. *Ecol. Monogr.*, 75, 435–450.

Legendre, P. & Gallagher, E.D. (2001). Ecologically meaningful transformations for ordination of species data. *Oecologia*, 129, 271–280.

Leibold, M.A., Holyoak, M., Mouquet, N., Amarasekare, P., Chase, J.M., Hoopes, M.F., *et al.* (2004). The metacommunity concept: a framework for multi-scale community ecology. *Ecol. Lett.*, 7, 601–613.

Lenth, R. (2023). emmeans: Estimated Marginal Means, aka Least-Squares Means_. *R package version 1.8.5*.

Leray, M. & Knowlton, N. (2015). DNA barcoding and metabarcoding of standardized samples reveal patterns of marine benthic diversity. *Proc. Natl. Acad. Sci. U. S. A.*, 112, 2076–2081.

Leray, M., Yang, J.Y., Meyer, C.P., Mills, S.C., Agudelo, N., Ranwez, V., *et al.* (2013). A new versatile primer set targeting a short fragment of the mitochondrial COI region for metabarcoding metazoan diversity: application for characterizing coral reef fish gut contents. *Front. Zool.*, 10, 34.

Lesser, M.P., Slattery, M. & Leichter, J.J. (2009). Ecology of mesophotic coral reefs. *J. Exp. Mar. Bio. Ecol.*, 375, 1–8.

Lett, C., Nguyen-Huu, T., Cuif, M., Saenz-Agudelo, P. & Kaplan, D.M. (2015). Linking local retention, self-recruitment, and persistence in marine metapopulations. *Ecology*, 96, 2236–2244.

Lett, C., Verley, P., Mullon, C., Parada, C., Brochier, T., Penven, P., *et al.* (2008). A Lagrangian tool for modelling ichthyoplankton dynamics. *Environ. Model. Softw.*, 23, 1210–1214.

Limer, B.D., Bloomberg, J. & Holstein, D.M. (2020). The Influence of Eddies on Coral Larval Retention in the Flower Garden Banks. *Frontiers in Marine Science*, 7.

Lin, H. & Peddada, S.D. (2024). Multigroup analysis of compositions of microbiomes with covariate adjustments and repeated measures. *Nat. Methods*, 21, 83–91.

Liu, G., Bracco, A., Quattrini, A.M. & Herrera, S. (2021). Kilometer-Scale Larval Dispersal Processes Predict Metapopulation Connectivity Pathways for Paramuricea biscaya in the Northern Gulf of Mexico. *Frontiers in Marine Science*.

Lopera, L., Bracco, A. & Herrera, S. (2025). Physical connectivity between mesophotic areas in the northern Gulf of Mexico. *J. Geophys. Res. Oceans*, 130, e2024JC021753.

Loya, Y., Eyal, G., Treibitz, T., Lesser, M.P. & Appeldoorn, R. (2016). Theme section on mesophotic

coral ecosystems: advances in knowledge and future perspectives. *Coral Reefs*, 35, 1–9.

Martin, M. (2011). Cutadapt removes adapter sequences from high-throughput sequencing reads. *EMBnet J.*, 17, 10.

Mayorga-Martínez, M., Bello-Pineda, J., Perales-Valdivia, H., Pérez-España, H. & Heyman, W.D. (2021). Characterizing Geomorphology of Mesophotic Coral Reef Ecosystems in the Southwestern Gulf of Mexico: Implications for Conservation and Management. *Frontiers in Marine Science*, 8.

McCartin, L., Saso, E., Vohsen, S.A., Pittoors, N., Demetriades, P., McFadden, C.S., *et al.* (2024). Nuclear eDNA metabarcoding primers for anthozoan coral biodiversity assessment. *PeerJ*, 12, e18607.

McClain, C.R., Hanks, G., Copley, S., Bryant, S.R.D. & Schubert, B.A. (2024). Macrofaunal Biodiversity and Patch Mosaics on the Deep Gulf of Mexico Seafloor. *Mar. Ecol.*, e12836.

McClain, C.R., Stegen, J.C. & Hurlbert, A.H. (2012). Dispersal, environmental niches and oceanic-scale turnover in deep-sea bivalves. *Proc. Biol. Sci.*, 279, 1993–2002.

Mcgrail, D. & Carnes, M. (1983). Shelfedge dynamics and the nepheloid layer in the northwestern gulf of Mexico.

Menegotto, A., Dambros, C.S. & Netto, S.A. (2019). The scale-dependent effect of environmental filters on species turnover and nestedness in an estuarine benthic community. *Ecology*, 100, e02721.

Menge, B.A. & Sutherland, J.P. (1987). Community regulation: Variation in disturbance, competition, and predation in relation to environmental stress and recruitment. *Am. Nat.*, 130, 730–757.

Meyer, K., Young, C., Sweetman, A., Taylor, J., Soltwedel, T. & Bergmann, M. (2016). Rocky islands in a sea of mud: biotic and abiotic factors structuring deep-sea dropstone communities. *Marine Ecology Progress Series*, 556, 45–57.

Montgomery, A.D., Fenner, D., Kosaki, R.K., Pyle, R.L., Wagner, D. & Toonen, R.J. (2019). American Samoa. In: *Coral Reefs of the World*. Springer International Publishing, Cham, pp. 387–407.

Morgan, K.M., Perry, C.T., Arthur, R., Williams, H.T.P. & Smithers, S.G. (2020). Projections of coral cover and habitat change on turbid reefs under future sea-level rise. *Proc. Biol. Sci.*, 287, 20200541.

Morrissey, D., Lim, A., Howell, K.L., White, M., Wheeler, A.J. & Allcock, A.L. (2023). The North-east Atlantic margin: A review of the geology, geography, oceanography, and vulnerable megabenthic ecosystems of the continental slope of Ireland and the United Kingdom. In: *Oceanography and Marine Biology*. CRC Press, Boca Raton, pp. 219–291.

Mullineaux, L.S., Metaxas, A., Beaulieu, S.E., Bright, M., Gollner, S., Grupe, B.M., *et al.* (2018). Exploring the ecology of deep-sea hydrothermal vents in a metacommunity framework. *Front. Mar. Sci.*, 5.

National Oceanic and Atmospheric Administration. (2021). Expansion of Flower Garden Banks National Marine Sanctuary. *Federal Register*.

Noaa, N. (2006). 2-minute gridded global relief data (etopo2) v2. *Natl Geophys Data Center, NOAA Natl Centers Env Inf*.

Norkko, J., Norkko, A., Thrush, S.F., Valanko, S. & Suurkuukka, H. (2010). Conditional responses to increasing scales of disturbance, and potential implications for threshold dynamics in soft-sediment communities. *Mar. Ecol. Prog. Ser.*, 413, 253–266.

Nurk, S., Meleshko, D., Korobeynikov, A. & Pevzner, P.A. (2017). metaSPAdes: a new versatile metagenomic assembler. *Genome Res.*, 27, 824–834.

Oksanen, J., Simpson, G., Blanchet, F.G., Kindt, R., Legendre, P., Minchin, P., *et al.* (2022). vegan community ecology package version 2.6-2 April 2022. *The Comprehensive R Archive Network. Available online: http://cran. r-project. org (accessed on 15 August 2022)*.

Pante, E. & Simon-Bouhet, B. (2013). marmap: A package for importing, plotting and analyzing bathymetric and topographic data in R. *PLoS One*, 8, e73051.

Pearman, J.K., Leray, M., Villalobos, R., Machida, R.J., Berumen, M.L., Knowlton, N., *et al.* (2018). Cross-shelf investigation of coral reef cryptic benthic organisms reveals diversity patterns of the hidden majority. *Sci. Rep.*, 8, 8090.

Peres-Neto, P.R., Legendre, P., Dray, S. & Borcard, D. (2006). Variation partitioning of species data matrices: estimation and comparison of fractions. *Ecology*, 87, 2614–2625.

Piredda, R., Tomasino, M.P., D'Erchia, A.M., Manzari, C., Pesole, G., Montresor, M., *et al.* (2017). Diversity and temporal patterns of planktonic protist assemblages at a Mediterranean Long Term Ecological Research site. *FEMS Microbiol. Ecol.*, 93, fiw200.

Pyle, R.L. & Copus, J.M. (2019). Mesophotic coral ecosystems: Introduction and overview. In: *Coral Reefs of the World*. Springer International Publishing, Cham, pp. 3–27.

Quinlan, A.R. & Hall, I.M. (2010). BEDTools: a flexible suite of utilities for comparing genomic features. *Bioinformatics*, 26, 841–842.

Ransome, E., Geller, J.B., Timmers, M., Leray, M., Mahardini, A., Sembiring, A., *et al.* (2017). The importance of standardization for biodiversity comparisons: A case study using autonomous reef monitoring structures (ARMS) and metabarcoding to measure cryptic diversity on Mo'orea coral reefs, French Polynesia. *PLOS ONE*.

Reimer, J.D., Kise, H., Santos, M.E.A., Lindsay, D.J., Pyle, R.L., Copus, J.M., *et al.* (2019). Exploring the Biodiversity of Understudied Benthic Taxa at Mesophotic and Deeper Depths: Examples From the Order Zoantharia (Anthozoa: Hexacorallia). *Frontiers in Marine Science*, 6.

Rezak, R., Bright, T.J. & Mcgrail, D. (1985). Reefs and banks of the northwestern Gulf of Mexico: Their geological, biological, and physical dynamics.

Rezak, R., Gittings, S.R. & Bright, T.J. (1990). Biotic assemblages and ecological controls on reefs and

banks of the northwest gulf of Mexico. *Am. Zool.*, 30, 23–35.

Riisgård, H.U. & Larsen, P.S. (2010). Particle capture mechanisms in suspension-feeding invertebrates. *Mar. Ecol. Prog. Ser.*, 418, 255–293.

Rocha, L.A., Pinheiro, H.T., Shepherd, B., Papastamatiou, Y.P., Luiz, O.J., Pyle, R.L., *et al.* (2018). Mesophotic coral ecosystems are threatened and ecologically distinct from shallow water reefs. *Science*, 361, 281–284.

Rodil, I.F., Lucena-Moya, P. & Lastra, M. (2018). The importance of environmental and spatial factors in the metacommunity dynamics of exposed Sandy Beach benthic invertebrates. *Estuaries Coast.*, 41, 206–217.

Saeedi, H., Warren, D. & Brandt, A. (2022). The environmental drivers of benthic fauna diversity and community composition. *Front. Mar. Sci.*, 9, 804019.

Salamanca-Díaz, D.A., Horkan, H.R., García-Castro, H., Emili, E., Salinas-Saavedra, M., Pérez-Posada, A., *et al.* (2025). The Hydractinia cell atlas reveals cellular and molecular principles of cnidarian coloniality. *Nat. Commun.*, 16, 2121.

Sammarco, P.W., Nuttall, M.F., Beltz, D., Hickerson, E.L. & Schmahl, G.P. (2016). Patterns of Mesophotic Benthic Community Structure on Banks Off vs Inside the Continental Shelf Edge, Gulf of Mexico. *Gulf Mex. Sci.*, 33, 7.

Sanchez, P.J., Dance, M.A., Kraus, R.T., Hill, R.L. & Rooker, J.R. (2023). Fish community characterization of mid-shelf and shelf- edge mesophotic coral ecosystems in the expanded Flower Garden Banks National Marine Sanctuary. *Bull. Mar. Sci.*, 99, 41–50.

Schmahl, G.P., Hickerson, E.L. & Precht, W.F. (2008). Biology and Ecology of Coral Reefs and Coral Communities in the Flower Garden Banks Region, Northwestern Gulf of Mexico. In: *Coral Reefs of the USA* (eds. Riegl, B.M. & Dodge, R.E.). Springer Netherlands, Dordrecht, pp. 221–261.

Semmler, R.F., Hoot, W.C. & Reaka, M.L. (2017). Are mesophotic coral ecosystems distinct communities and can they serve as refugia for shallow reefs? *Coral Reefs*, 36, 433–444.

Shen, W., Le, S., Li, Y. & Hu, F. (2016). SeqKit: A cross-platform and ultrafast toolkit for FASTA/Q file manipulation. *PLoS One*, 11, e0163962.

Studivan, M.S. & Voss, J.D. (2018). Assessment of Mesophotic Coral Ecosystem Connectivity for Proposed Expansion of a Marine Sanctuary in the Northwest Gulf of Mexico: Population Genetics. *Frontiers in Marine Science*, 5.

Tamborrino, L., Titschack, J., Wienberg, C., Purkis, S., Eberli, G.P. & Hebbeln, D. (2022). Spatial distribution and morphometry of the Namibian coral mounds controlled by the hydrodynamic regime and outer-shelf topography. *Front. Mar. Sci.*, 9.

Tragin, M., Zingone, A. & Vaulot, D. (2018). Comparison of coastal phytoplankton composition

estimated from the V4 and V9 regions of the 18S rRNA gene with a focus on photosynthetic groups and especially Chlorophyta. *Environ. Microbiol.*, 20, 506–520.

Tunnell, J.W. (2007). Coral reefs of the southern Gulf of Mexico.

Turner, J.A., Babcock, R.C., Hovey, R. & Kendrick, G.A. (2017). Deep thinking: a systematic review of mesophotic coral ecosystems. *ICES J. Mar. Sci.*, 74, 2309–2320.

Vasbinder, K., Ainsworth, C.H., Liu, Y. & Weisberg, R.H. (2023). Gulf of Mexico larval dispersal: Combining concurrent sampling, behavioral, and hydrodynamic data to inform end-to-end modeling efforts through a Lagrangian dispersal model. *Deep Sea Res. Part 2 Top. Stud. Oceanogr.*, 211, 105323.

Villalobos, R., Aylagas, E., Ellis, J.I., Pearman, J.K., Anlauf, H., Curdia, J., *et al.* (2024). Responses of the coral reef cryptobiome to environmental gradients in the Red Sea. *PLoS One*, 19, e0301837.

Villalobos, R., Aylagas, E., Pearman, J.K., Curdia, J., Lozano-Cortés, D., Coker, D.J., *et al.* (2022). Inter-annual variability patterns of reef cryptobiota in the central Red Sea across a shelf gradient. *Sci. Rep.*, 12, 16944.

Voss, J., Williams, M., Reed, J. & Clark, R. (2014). Benthic and fish communities in the mid and lower mesophotic zone of the sanctuary. *National Marine Sanctuary ….*

Williams, I.D., Couch, C.S., Beijbom, O., Oliver, T.A., Vargas-Angel, B., Schumacher, B.D., *et al.* (2019). Leveraging Automated Image Analysis Tools to Transform Our Capacity to Assess Status and Trends of Coral Reefs. *Frontiers in Marine Science*, 6.

Wilson, A.M., Raine, R., Mohn, C. & White, M. (2015). Nepheloid layer distribution in the Whittard Canyon, NE Atlantic Margin. *Mar. Geol.*, 367, 130–142.

Wolfe, K., Desbiens, A.A. & Mumby, P.J. (2023). Emigration patterns of motile cryptofauna and their implications for trophic functioning in coral reefs. *Ecol. Evol.*, 13, e9960.

Wolfe, K., Desbiens, A., Stella, J. & Mumby, P.J. (2020). Length–weight relationships to quantify biomass for motile coral reef cryptofauna. *Coral Reefs*, 39, 1649–1660.

Zhou, X., Lopera, L., Roa-Varón, A. & Bracco, A. (2024). Modeling the larval dispersal and connectivity of Red Snapper (Lutjanus campechanus) in the Northern Gulf of Mexico. *Prog. Oceanogr.*, 224, 103265.

Zimmerman, T.L. & Martin, J.W. (2004). Artificial Reef Matrix Structures (Arms): An Inexpensive and Effective Method for Collecting Coral Reef-Associated Invertebrates. *Gulf Caribb. Res.*, 16, 59–64.

Supplementary Information

Supporting Methods

Site selection and deployment strategy

Thirty-six Autonomous Reef Monitoring structures were deployed for two years across six reef banks within and adjacent to the Flower Garden Banks National Marine Sanctuary (FGBNMS): Stetson, East Flower Garden Bank, Bright, McGrail, Alderdice, and Diaphus. Site selection was based on previous extensive ROV surveys of coral communities on the Texas-Louisiana continental shelf, multibeam bathymetric maps, and management priorities relevant to sanctuary expansion alternatives that were approved during the ARMS deployment period. Within each bank, ARMS were deployed between 54-85 m depth within the Coralline Algae Zone characterized by algal nodules and rocky outcrops that host octocorals, antipatharians, and sponges (Schmahl *et al.* 2008). Sites were strategically selected to capture habitat variability across depth gradients, substrate, and coral abundance, with deployment density varying by bank based on habitat availability. Initially, ARMS were deployed at two depth ranges within a bank, and within the deeper depths, ARMS were deployed either within coral communities ("coral") or approximately 10m away in areas with minimal coral cover ("background") consisting of primarily rubble and sand substrate. At each site locality, three ARMS were deployed as spatial replicates in close proximity to one another to account for small-scale variability in recruitment and colonization patterns. However, preliminary analysis revealed no significant ecological differences between coral and background localities at deeper depths. Consequently, site designations were revised to reflect depth-based categories: shallow, deep1, and deep2. This approach ensured that ARMS placements would complement existing monitoring efforts while providing ecological connectivity data relevant to marine protected area network design and coral ecosystem conservation in this region.

Benthic Community Sampling

Prior to ARMS recovery, two to four replicate samples were collected using 1.7L General Oceanics Niskin bottles (Model 1010) mounted on the ROV *Global Explorer.* Seawater was filtered through 0.22µm Sterivex filters, processed, and preserved following protocols detailed in (McCartin *et al.* 2024). ARMS were then recovered using the ROV and 45µm mesh-lined crates, ensuring that all motile fauna remained with the ARMS unit. Upon recovery, each ARMS was held in a large cooler containing filtered and chilled seawater until they were processed. ARMS were then transferred to another container with filtered seawater and disassembled plate-by-plate following Ransome et al. (2017) (Ransome *et al.* 2017) . Each plate was removed from the structure and gently sifted to capture any motile fauna and sediment into the holding water. Seawater in this holding container was then sieved to separate motile

organisms and sediment into three size fractions: >2mm; 500µm -2mm (500µm fraction), and 106µm-500µm (100µm fraction). Organisms larger than 2mm were sorted, photographed, and processed as reference library voucher specimens. The two 100µm and 500µm size fractions were preserved in 95% EtOH and represent the "motile" fractions. Prior to DNA extraction, motile fractions underwent decantation to separate organic matter from sediments. Each fraction was transferred to a flask, diluted with deionized water, and vigorously shaken to suspend organic particles. The mixture was then poured through appropriate sieves (100µm for the 500µm-2mm fraction and 45µm for the 106µm-500µm fraction) to separate floating organic matter from heavier sediments. This decantation process was repeated until only sediments remained in the flask. The collected organic matter was homogenized using a mortar and pestle, and preserved in 95% ethanol until DNA extraction. Each plate was photographed, representative sessile organisms were subsampled for reference library vouchers, and then all sessile organisms were scraped off the plates and blended into a homogeneous mixture. This mixture will hereby be referred to as the "sessile" fraction. Filtered surface seawater from the ARMS holding containers was collected as a negative control and filtered over a 0.22µm polyethersulfone Sterivex filter to assess potential contamination during processing.

Environmental and Spatial Factors

HOBO Environmental data loggers were attached to one ARMS at each site and recorded dissolved oxygen, light, salinity, and/or temperature over the total time ARMS were deployed (HOBO MX2204, MX2203, UA-002-08, U26-001). Water column visibility, an inverse proxy for turbidity and nepheloid layer intensity, was estimated from ROV 4K video footage at each site by eight experienced scuba divers who were blinded to the location and depth of each site. Low power parallel lasers mounted 10 cm apart provided a consistent scaling reference to calibrate visibility estimates. All recoveries occurred during the day, ensuring similar daylight conditions for all estimates. Raw visibility estimates (meters) were standardized using the formula $(visibility\ estimate\ -\ mean\ estimate\ per\ diver\ across\ all\ sites)/SD\ of\ the\ diver\ means$, then ranked from 1 (clearest conditions) to 13 (most turbid). The mean standardized rank across all divers was calculated for each site and used as the turbidity variable in subsequent analyses.

Satellite-derived oceanographic variables were obtained from the publicly available Global Ocean Colour (Copernicus-GlobColour) database at a 4km resolution for the study region. Variables included chlorophyll-a concentration (CHL), the absorption coefficient of dissolved and detrital matter (CDM), suspended particulate matter (SPM), backscattering coefficient (BBP), and surface primary productivity (PP). To identify collinear variables, we conducted principal component analysis (PCA) on the full environmental matrix. CHL, SPM, and BBP were highly correlated with PP (primary axis of PCA

variation); therefore, PP was retained as the representative variable for surface productivity while the correlated variables were excluded. Similarly, bottom temperature was strongly correlated with depth across our sites, as expected from thermocline structure and vertical temperature stratification in the water column. We retained depth as the primary bathymetric predictor, as it serves as a proxy for multiple co-varying depth associated factors including temperature, light attenuation, hydrostatic pressure, and other depth-dependent environmental gradients characteristic of mesophotic reef ecosystems (Pyle & Copus 2019). The final non-collinear environmental variable dataset included depth, turbidity (standardized visibility rank), and primary productivity.

Environmental variables exhibited spatial structure across the study region, with PP strongly associated with longitude (eastward gradient, r + 0.93) and turbidity associated with latitude (northward intensification of the benthic nepheloid layer). This spatial structuring reflects regional oceanographic processes, including a far-field nutrient influence from the Mississippi River and shelf-scale sediment transport patterns. Consequently, PP functions as an environmental variable (phytoplankton biomass affecting food availability) as well as a spatial variable (longitudinal position). To avoid overparameterization and collinearity issues, we included PP selectively in PERMANOVA models: baseline environmental models included only depth and turbidity (the primary environmental gradients directly relevant to mesophotic communities), while extended models included PP to test for productivity effects and interactions with spatial variables. This approach allowed us to distinguish between pure environmental filtering (depth + turbidity), productivity-mediated effects, and spatial structure independent of measured environmental gradients. For sessile-associated metabarcoding (18S/COI ARMS) and coverage (CoralNet), PP was initially excluded from final models. While exploratory conditional tests showed statistically significant effects independent of longitude (PP | longitude: R3 = 0.05-0.08, $p < 0.001$ across size fractions), we excluded PP due to severe multicolinearity with longitude (VIF>10), making it impossible to distinguish genuine productivity effects from spatial position. Spatial predictors were included across all datasets to test for geographic structure independent of measured environmental gradients, with significant spatial effects after conditioning on environment interpreted as evidence for dispersal limitation

DNA extraction, metabarcoding library preparation, and sequencing

DNA from ARMS samples were extracted from the sessile and motile fractions using the Qiagen DNeasy PowerMax Soil Kit following Ransome et al. (2017), followed by a salt precipitation was used to concentrate the 5ml DNA extract to 100 µl. Niskin eDNA samples were extracted following protocols detailed in (McCartin *et al.* 2024). Marine eukaryotic diversity was assessed by amplifying cytochrome oxidase subunit I (COI) and 18S V4 loci. COI was amplified using mlCOIintF/jgHCO2198 primers

(GGWACWGGWTGAACWGTWTAYCCYCC/TAIACYTCIGGRTGICCRAARAAYCA) (Geller *et al.* 2013; Leray *et al.* 2013), and the 18S V4 region was targeted using V4_18SNext.For and V4_18SNext.Rev primers (TCGTCGGCAGCGTCAGATGTGTATAAGAGACAG/GTCTCGTGGGCTCGGAGATCTGTATAAGAGACAG) (Piredda *et al.* 2017; Tragin *et al.* 2018). For COI, 25 µl PCR reactions included 2 µl DNA template, 5 µl 5× Q5U reaction buffer, 1.25 µl of each primer, 1 µl BSA, 0.5 µl 10 mM dNTPs, 0.25 µl New England Biolabs Q5U Hot Start High-Fidelity DNA polymerase (NEBM0515), and 13.75 µl nuclease-free water. A touchdown thermocycling protocol consisted of an initial denaturation at 98°C for 2 min, 16 touchdown cycles (98°C for 10 s, 62°C for 30 s, decreasing by 1°C per cycle, and 72°C for 60 s), followed by 20 additional cycles (98°C for 10 s, 46°C for 30 s, 72°C for 60 s), and a final extension at 72°C for 2 min. For 18S, 25 µl PCR reactions included 2.5 ng DNA template, 5 µl 5× HF DNA buffer, 1.25 µl of each primer, 2.5 µl dNTPs, 1 U Phusion DNA polymerase, and 13.5 µl nuclease-free water. Amplification used an initial denaturation at 98°C for 30 s, 10 touchdown cycles (98°C for 10 s, 44°C for 30 s, decreasing by 1°C per cycle, and 72°C for 15 s), followed by 15 additional cycles (98°C for 10 s, 62°C for 30 s, 72°C for 15 s), and a final extension at 72°C for 7 min. Triplicate PCR reactions were performed per sample, pooled, and verified via agarose gel electrophoresis (~318 bp band for COI, ~380-470 bp for 18S). Each Autonomous Reef Monitoring Structure (ARMS) unit contributed nine samples (sessile fraction, 100 µm fraction, and 500 µm fraction) for analysis. Pooled PCR products were sent to Rush Genomics and Microbiome Core Facility (Chicago, USA) for amplicon library preparation and sequencing on the Illumina MiSeq platform.

Sessile and motile vouchers were sequenced via both Sanger capillary sequencing and shallow whole genome sequencing (genome skimming) to generate a COI and 18S barcode reference library. DNA from 95% ethanol-preserved vouchers was isolated via phenol-chloroform extraction on an Autogenprep 965. For Sanger sequencing, the Folmer region of COI was was amplified using Geller primers: jgLCO1490 (forward) TITCIACIAAYCAYAARGAYATTGG and jgHCO2198 (reverse) TAIACYTCIGGRTGICCRAARAAYCA (Geller et al. 2013). 1.0 ul template DNA was amplified in 10 ul PCR reactions utilizing 5.0 ul nuclease-free water, 3.3 ul Promega GoTaq Hot Start Master Mix (PM7433), 0.1 ul BSA, and 0.3 ul 10 uM primers using the following thermocycling protocol: initial denaturation at 95°C for 5 min, followed by 4 cycles of 94°C for 30 s, 50°C for 45 s, and 72°C for 1 min, then 34 cycles of 94°C for 30 s, 45°C for 45 s, and 72°C for 1 min, and a final extension at 72°C for 8 min. PCR product was verified via agarose gel electrophoresis and cleaned using Applied Biosystems ExoSAP-IT Express (75001). PCR products were cycle sequenced in single directions using Applied Biosystems BigDye reagents, 10uM forward or reverse primer, and 30 cycles of 95°C for 30 s, 50°C for 30 sec, and 60°C for 4 min. Unincorporated dye was cleaned from cycle sequencing reactions via

Sephadex filtration and reactions were sequenced on an ABI 3730xl (96-capillary) sequencer. Traces assembled and QAQC'd in Geneious 2023.0.1. Genome skimming was performed on representative individuals from each distinct COI lineage and vouchers that failed Sanger sequencing. For genome skimming, DNA extractions were quantified with the Quant-IT HS assay kits on the SpectraMax ID3 microplate reader. Up to 10 ng DNA per sample was prepared using the NEB Next Ultra II FS DNA Library Prep Kit following manufacturer's protocols with modifications as in Hoban et al. (Hoban *et al.* 2022), a 3 minute enzymatic fragmentation time, and automated bead cleanup via the Opentrons pipetting system. Genetic sample metadata was recorded in the Genomics Observatories Metadatabase (GeOMe) (https://n2t.net/ark:/21547/EBk2) and sequences in GenBank (BioProject XXX).

Bioinformatics

Reads were demultiplexed and assessed for quality using *FASTQC* (Andrews & Others 2010) and summarized with *MultiQC* (Andrews & Others 2010; Ewels *et al.* 2016). Adapter sequences and primers were removed using cutadapt (Martin 2011). Reads were filtered and trimmed based on quality scores using *DADA2* (Callahan *et al.* 2015). Filtered reads were dereplicated and amplicon sequencing variants (AVSs) were inferred using the *DADA2* error model. Chimeric sequences were identified and removed with removeBimeraDenovo. Post-clustering curation was performed using *LULU (Frøslev et al. 2017)* with marker-specific parameters: for COI, minimum_math = 97%, minimum_relative_cooccurence = 0.95, minimum_ratio_type = "min", and minimum_ratio = 2; for 18S, minimum_math = 99.5%, minimum_relative_cooccurence = 0.95, minimum_ratio_type = "min", and minimum_ratio = 2. For taxonomic assignment of amplicon sequence variants (ASVs), we employed a custom hierarchical taxonomy pipeline that leveraged multiple reference databases in a prioritized approach. ASVs from both COI and 18S markers were taxonomically classified using a three-tier reference system in full mode, incorporating NMNH voucher specimens, MetaZooGene marine references, and the NCBI nucleotide database.This hierarchical approach address the well-documented challenge of limited reference barcode data in public databases, which often results in high numbers of unidentified sequences in marine metabarcoding studies (Leray & Knowlton 2015). Sequences were compared against all three databases using BLAST with marker-specific thresholds of 85% identity, minimum alignment length of 200bp for COI and 300bp for 18S (Ransome *et al.* 2017). For each ASV, the best taxonomic assignment was selected based on a strict database prioritization order (NMNH > MZG > NCBI), which prioritized highly curated voucher specimens and specialized marine databases over more general repositories, even when lower-priority databases showed higher sequence identity. This approach ensured that taxonomic assignments leveraged the most reliable reference sources first. Post-assignment processing included backfilling missing taxonomy ranks using the World Register of Marine Species (WoRMS) API, filtering

out non-marine organisms, and forward-filling missing ranks with standardized notation. Environmental sequences and problematic assignments were automatically removed, and metazoan taxa were optionally separated from non-metazoan taxa for targeted ecological analysis. This multi-database, priority-driven approach enabled consistent and reliable taxonomy assignment across both markers while maximizing the use of curated reference databases.

For genome skimmed voucher specimen references, raw reads were first assessed with *FASTQC,* followed by processing with *FASTP (Chen et al. 2018)* and *Trimmomatic (Bolger et al. 2014)*. Trimmed reads were mapped against human and PhiX genomes with *BOWTIE2* (Langmead & Salzberg 2012) to remove common contaminants. To assemble COI and 18S barcodes, cleaned reads were aligned against BOLD, SILVA SSU, and SILVA LSU databases with *BBMap ("BBMap" 2022)*. Read pairs were assembled with *MetaSPAdes* (Nurk *et al.* 2017) using default settings. Taxonomic identity for assembled contigs were determined using BLASTN and longest alignment region for the target organism was extracted using *BEDTools* (Quinlan & Hall 2010) and SeqKit (Shen *et al.* 2016). For eukaryotic 18S rRNA genes, *Barrnap* (https://github.com/tseemann/barrnap) was run on metagenomic assemblies produced in *MetaSPAdes*, candidate contigs were checked via BLASTN, and longest matching 18S retained.

Annotation of Plate Photographs

Sessile recruits on all ARMS plates were photographed and annotated using the semi-automanted web-based platform, CoralNet (Beijbom 2015; Beijbom *et al.* 2015; Chen *et al.* 2021; Williams *et al.* 2019). Each plate image was manually scored to establish machine learning training data, followed by semi-automated classification of all remaining plate images. All automatically generated annotations underwent manual verification to maintain data quality. We used a comprehensive labelset encompassing hard corals, octocorals, hydrozoans, sponges, erect and encrusting bryozoans, solitary and colonial tunicates, mollusks, worm tubes, crustose coraline algae, red, brown, green algaes, sediment, bacterial biofilms, no recruitment, unavailable, and unknown. This expanded classification captured cryptobenthic community diversity while maintaining compatibility with standard ARMS protocols. We used a uniform grid of 15 x 15 points. Coralnet annotations were compared to COI and 18S metabarcoding data at the phylum level (Annelida, Bryozoa, Chlorophyta, Chordata, Forminifera, Hemichordata, Hydrozoa, Cnidaria, Mollusca, Porifera, and Rhodophyta).

Hydrodynamic Larval Dispersal Models

We employed the Coastal and Regional Ocean Community model (CROCO) in its hydrostatic configuration to simulate ocean conditions during the summer season from 2014 to 2016 (Auclair *et al.*

2019), years that captured significant variability in regional oceanographic conditions, including different configurations of the Loop Current and presence of mesoscale eddies of various sizes. Multiple benthic invertebrates within the study region, including sceractinians, anipatharian, and ocotcorals, undergo gametogensis and spawning during late summer (July-October). This timing aligns with peak thermal stability and current-driven larval transport conditions that enhance recruitment potential (Garavelli *et al.* 2018; Holstein *et al.* 2015; Johnstone *et al.* 2025; Salamanca-Díaz *et al.* 2025; Sammarco *et al.* 2016). The model domain extended from 24°N to 31°N and 98°W to 82°W, with a 1 km horizontal resolution and 50 sigma-layers in the vertical, providing enhanced resolution near the ocean bottom. The model grid was built based on 2-min Gridded Global Relief Data (ETOPO2) topography. CROCO was forced every three hours with atmospheric data from the Navy Global Environmental Model (NAVGEM), and it was nudged at the boundaries to the Hybrid Coordinate Ocean Model – Navy Coupled Ocean Data Assimilation (HYCOM-NCODA) analysis system (Cummings 2005; Cummings & Smedstad 2013; Noaa 2006). Furthermore, the TPXO-7 global tidal model was used to include the most important tidal components (M2, S2, N2, K2, K1, O1, P1, Q1, Mf, and Mm)(Egbert & Erofeeva 2002). Three-dimensional hydrodynamic fields were saved every 30 min. This configuration has been previously used to assess the dispersal patterns of Red Snapper larvae (Zhou *et al.* 2024) and connectivity between areas known to be populated by mesophotic corals (Lopera *et al.* 2025). Further details on model validation at different levels of the water column can be found in Lopera et al. (Lopera *et al.* 2025). We used the Lagrangian tool Ichthyop v3.3.16 to simulate the three-dimensional advection of particles during August 2014, 2015, and 2016 (Lett *et al.* 2008). 40,000 particles were released 50 cm above the ocean bottom within an area of approximately 5 km² surrounding the sampling locations twice in each year, on the 3rd and 13th of August, and were followed for 20 and 40 days. Three types of scenarios were implemented to represent a broad range of species within the mesophotic zone: a passive scenario, in which horizontal and vertical advection by the flow fields determines the particle advection at all times under the assumption that the larvae are neutrally or slightly negatively buoyant throughout their life; and two OVM (ontogenic vertical migration) scenarios, in which it assumed that the larvae are buoyant for two (OVM-2) or ten (OVM-10) days after their release. After this initial time the larvae are returned near the ocean bottom according to their release depths under the assumption that they become neutrally buoyant with respect to the ARMS - and their release - depths. This approach simulates a biological trait exhibited by many marine species, in which larvae have a large fat content at release time and individuals migrate vertically to preferred depth ranges at later developmental stages. The implementation of the OVM trait followed what was proposed in Zhou et al. (Zhou *et al.* 2024).

Local retention was not presented as it would artificially appear inflated due to model constraints. Because of the model grid resolution and the Courant-Friedrichs-Lewy (CFL) criterion necessary for

numerical stability, all simulated larvae inevitably spend at least a few time steps within the same grid points where release occurred. Larvae were released over several kilometers around each site, which would result in nearly 100% local recruitment by design at all sites. Additionally, no-precompetency phase was considered in our connectivity assessments, as our research focuses primarily on broader-scale larval transport patterns between distinct populations rather than self-recruitment dynamics within individual sites.

Statistical Analysis

Data Transformation for Community Analyses

Multiple transformations were evaluated prior to calculating Bray-Curtis similarity matrices for beta diversity analyses to address numerically dominant taxa overwhelming community patterns in amplicon sequencing data. Untransformed data, Hellinger transformation (square root of relative abundances), and fourth root transformation were compared using NMDS stress values as the selection criterion. The fourth-root transformation produced the lowest NMDS stress (0.184) compared to Hellinger transformation (0.203) and untransformed data (0.247), indicating improved representation of community dissimilarity in reduced dimensions. The fourth-root transformation down-weights abundant taxa while preserving more quantitative information, making it appropriate for revealing community-wide patterns in the highly skewed abundance distributions typical of metabarcoding datasets (Anderson *et al.* 2006; Legendre & Gallagher 2001). For metabarcoding datasets (COI-ARMS, 18S-ARMS, 18S-eDNA), fourth root transformation was applied to two separate data matrices depending on the analysis: (1) rarefied ASV count data for NMDS ordination, and (2) non-rarefied ASV count data for all beta diversity analyses. This dual approach balanced the need to control for sequencing depth variation in ordination visualization (rarefied) while maximizing statistical power for hypothesis testing (non-rarefied with total read counts as covariats where appropriate). For CoralNet percent coverage data, fourth root transformation was applied to the proportional abundance matrix to reduce the influence of dominant taxa (Clarke & Gorley 2015). The 2mm motile fauna abundance data (order-level counts) were not transformed, as sample sizes were modest (n=36) and we employed non-parametric correlation methods robust to distributional assumptions.

Alpha Diversity Metrics

Alpha diversity metrics were calculated for each sample across all datasets to capture different aspects of community structure: (1) observed richness (S), the number of unique taxonomic units (ASVs for molecular data, orders for 2mm visual surveys, phyla for CoralNet) present in each sample; (2) Shannon diversity (H'), calculated as $H' = -\sum p_i^2$, representing the probability of that two randomly selected individuals belong to different taxa; and (4) Pielou's evenness (J'), measuring how evenly

abundances are distributed among taxa independent of richness. Shannon and Simpson indices integrate both richness and evenness components and served as the primary diversity metrics for hypothesis testing, while richness and evenness were analyzed separately to mechanistically interpret diversity patterns. All diversity indicators were calculated using the *Diversity* function in the *Vegan* package v2.6-10 (Oksanen *et al.* 2022).

We employed dataset-specific statistical approaches tailored to the sampling design, taxonomic resolution, and sample size of each data type, prioritizing ecological appropriateness over methodological uniformity. For COI and 18S ARMS metabarcoding data, we used linear mixed-effects models (LMMs) to test effects of size fraction, environmental variables, and sampling location on alpha diversity while accounting for paired samples. All models included ARMS unit as a random intercept using the 'lmer' function in lmerTest v3.1-3 (Kuznetsova *et al.* 2017). Diversity metrics were calculated from rarefied data (COI: 7,285 reads per sample, the minimum library size, 18S: 17,000 reads per sample, retaining 82.7% of ASVs). Three complementary LMM analyses were conducted: (1) Size fraction effects tested our primary hypothesis that sessile (biofilm and encrusting organisms) and motile communities differ in diversity structure. Models included size fraction as a fixed effect: Diversity ~ fraction + (1|ARMS_ID). Type II Wald chi-square tests were performed using the 'Anova' function in Car v3.1-2 (Fox & Weisberg 2018) to assess overall fraction effects, followed by planned contrasts comparing sessile versus pooled motile fractions (100um + 500 um combined) using the emmeans package (Lenth 2023). No multiple comparison adjustment was applied to planned contrasts as these were a priori hypotheses. (2) Environmental gradient effects were evaluated to determine the influence of depth (meters below sea level) and turbidity (standardized rank from visibility estimates) on diversity while controlling for fraction effects: Diversity ~ depth + turbidity_std_rank + fraction + (1|ARMS_ID). Marginal R^2 values (variance explained by fixed effects only) were calculated using the r.squaredGLMM function in MuMin (Bartoń 2022) to quantify the proportion of diversity variance attributable to environmental gradients. (3) Spatial variation assessed heterogeneity in diversity across the 12 sampling sites: Diversity ~ fraction + sitelocality + (1|ARMS_ID). When overall site effects were significant ($\alpha = 0.05$), we performed post-hoc pairwise comparisons among sites using emmeans with Tukey adjustment for multiple comparisons and Kenward-Roger approximation for degrees of freedom. Model assumptions (linearity, homoscedasticity, normality of residuals) were verified by visual inspection of residual plots. One COI richness model showed boundary singular fit (random effect variance = 0), indicating minimal variation among size fractions from the same ARMS unit, but random effect structure was retained for consistency across metrics and datasets. This singularity suggests that size fraction and environmental effects account for most variation in richness, with negligible additional ARMS-specific variation.

For 18S eDNA metabarcoding data, general linear models were used to test effects of sampling location and environmental variables on alpha diversity. Sequential Niskin water collections represent technical replicates, therefore results were interpreted conservatively and did not conduct post-hoc pairwise comparisons unless main effects reached a stringent threshold ($\alpha = 0.01$). Site differences in diversity were tested using one-way ANOVA with Tukey's HSD post-hoc tests (when $\alpha < 0.01$). Environmental effects (depth, visibility rank, primary productivity) were assessed using multiple linear regression: Diversity ~ depth + visibility_rank + primary_productivity. Type II sums of squares (car package) was used to test individual predictors and calculated R^2 values to quantify variance explained while penalizing for the number of predictors. For CoralNet sessile recruit annotations and 2mm motile fauna collections, we employed descriptive statistics and non-parametric correlation analyses rather than formal hypothesis testing. These datasets differed fundamentally from molecular data in taxonomic resolution (Phylum or Order level for CoralNet, Order-level for 2mm fauna vs ASV-level for metabarcoding), sample sizes (n = 36 ARMS units), and the absence of paired or nested structure. Given these limitations, we prioritized effect sizes, confidence intervals, and biological patterns over significance testing. CoralNet diversity metrics were calculated from the proportional coverage of live organisms across taxonomic groups. We calculated descriptive statistics for each site and used Spearman rank correlation coefficients to examine relationships between diversity metrics and environmental gradients (depth, turbidity rank). Spearman correlation is appropriate for continuous environmental gradients and is robust to non-normal distributions and small sample sizes. Given the modest sample size of 2mm motile fauna counts, low taxonomic resolution, and lower diversity compared to molecular methods, we employed a descriptive approach emphasizing biological effect sizes rather than significant testing. Spearman and Kendall rank correlation coefficients (both robust to nonnormality) between diversity metrics and environmental variables. To quantify environmental patterns, samples were divided into turbidity terciles (Clear, Intermediate, Turbid) and ecologically meaningful depth groups (Shallow Mesophotic 54-66 m; Deep Mesophotic: 81-85m) based on natural depth transitions in the region. For each environmental grouping, descriptive statistics were calculated including medians, interquartile ranges (IQR), and ranges to characterize diversity patterns. Effect sizes were quantified between environmental extremes (Clear vs. Turbid; Shallow vs. Deep Mesophotic) using median differences and percentage changes, and range overlap between groups was assessed to evaluate the degree of environmental gradient separation.

Beta Diversity Analyses

Community patterns were visualized using non-metric multidimensional scaling (NMDS) based on Bray-Curtis dissimilarity matrices calculated from fourth root transformed data. For metabarcoding

datasets (COI-ARMS, 18S-ARMS, 18S-eDNA), NMDS was performed on rarefied ASV abundance data to control for sequencing depth variation in ordination space. For visual survey data (CoralNet, 2mm motile fauna), NMDS was performed on fourth root transformed count or percent cover data. NMDS was implemented using the metaMDS function in *Vegan* with k=2 dimensions, 1000 maximum iterations, and multiple random starts to ensure global solution convergence. Ordination plots were used for exploratory visualization of community patterns across environmental gradients and sampling sites. Permutational multivariate analysis of variance (PERMANOVA;(Anderson 2001)) to test effects of environmental, spatial, and local factors on community composition. All PERMANOVA analyses were performed on Bray-Curtis dissimilarity matrices calculated from fourth root transformed data. For metabarcoding datasets, we used non-rarefied ASV abundance data for PERMANOVA testing, as Bray-Curtis dissimilarity inherently accounts for differences in total abundance (sampling depth), and retaining the full dataset maximizes statistical power for hypothesis testing (McMurdie and Holmes 2014). Prior to PERMANOVA, we assessed multivariate homogeneity of group dispersions using PERMDISP (Anderson *et al.* 2006) implemented with the *betadisper* function. All PERMANOVA tests used 999 permutations and were implemented using the *adonis* function in vegan with Type I (sequential) sums of squares unless otherwise noted. Statistical significance was set at for all tests ($\alpha = 0.05$). To distinguish among environmental filtering, dispersal limitation, and unmeasured local processes, we employed hierarchical variance partitioning using conditional PERMANOVA tests. We conducted three types of analyses. First, marginal tests quantified individual variable effects tested separately (community-preditor). Second, combined models grouped related predictors to assess broad-scale patterns: environmental baseline (depth + turbidity), geographic combined (latitude + longitude), and full regional model (depth + turbidity + latitude + longitude). Third, conditional tests isolated pure effects via model comparison. Geography | Environment was calculated as R2 (Env + Geo) - R2 (Env) and represents spatial structure beyond environmental gradients, interpretable as dispersal limitation or unmeasured spatially-structured processes. Environment | Geography was calculated as R^2(Env + Geo) - R^2(Geo) and represents environmental effects beyond spatial autocorrelation. Site | All measurements were calculated as R^2(Full + Site) - R^2(Full). and captures site-specific variance beyond all regional predictors, including local heterogeneity, microhabitat complexity, or biological interactions. This framework partitions community assembly into regional environmental filtering, dispersal limitation, and local-scale processes operating at different spatial scales.

For COI and 18S ARMS metabarcoding datasets (n = 114 and 108 samples, respectively), we tested effects of depth, turbidity (continuous, derived from diver visibility estimate), latitude, longitude, and site locality on community composition. Analyses were conducted separately for five community subsets: all samples combined, sessile fraction only, motile fractions combined (100 µm + 500 µm

pooled), and each motile size class independently (100 µm only, 500 µm only). This factorial design tested whether environmental and spatial drivers differ between sessile (benthic recruitment) and motile communities, and whether size structure dispersal affects spatial patterns. For size fraction comparisons within ARMS units, we used restricted permutations (permuting within ARMS units only) to account for the paired structure of samples from the same ARMS. For 18S eDNA (n=33 samples), effects of depth, turbidity, primary productivity, and site locality on community composition. For visual survey datasets (plate image annotations, and motile fauna counts), we tested effects of depth, turbidity, primary productivity, latitude, longitude, and site locality on community composition. Plate image annotations examined proportional cover of 14 taxonomic groups (primarily phyla) derived from point annotations, while motile fauna analyses examined order-level abundance counts of organisms collected within each ARMS. Each ARMS unit was treated as an independent sample (n=36 for both datasets). Given the coarser taxonomic resolution (phylum or order level) and lower diversity of visual surveys compared to molecular methods, we interpreted PERMANOVA results from these datasets as exploratory, emphasizing effect sizes (R^2 values) over p-values.

Principal coordinated analysis (PCoA) was performed on Bray-Curtis dissimilarity matrices calculated from fourth-root transformed, non-ratified relative abundance data using *cmdscale* function in R. Analysis were conducted separately for all samples combined and for individual size fractions within each dataset. The percentage of variance explained by each ordination axis was calculated from the eigenvalues. Environmental and spatial correlations with PCoS axes were assessed using vector fitting (*envfit()* function, *vegan* package) with 999 permutations to test significance. Individual Spearman rank correlations between each environmental variable and the first four PCoA axes were calculated to quantify the strength and direction of relationships for each dataset. Distance-based redundancy analysis (dbRDA) was used to partition community variation among environmental and spatial factors using the *capscale()* function in package *vegan*. A hierarchical series of models was tested across all datasets: (1) individual environmental drivers tested separately (depth, turbidity rank), (2) combined environmental model (depth + turbidity), (3) spatial model (latitude + longitude), and (4 environmental + spatial model. For datasets including primary productivity (18S-eDNA, CoralNet, 2mm fauna), we tested an additional combined environmental model (depth + turbidity + PP mean). To isolate unique contributions to predictor sets, conditional analyses were conducted using the *Condition()* function, which partitions variance by fitting one set of predictors after removing variance explained by another set. Following (Legendre *et al.* 2005) and (Peres-Neto *et al.* 2006) we tested: (1) Spatial effects conditioned on environmental variables (geography | environment), interpreted as evidence for dispersal limitation when significant, (2) environmental effects conditioned on spatial variables (environment | geography), representing environmental filtering independent of spatial autocorrelation, and (3) site identity effects

after conditioning on all measured variables (site | environment + geography), capturing unmeasured local processes. We additionally tested turbidity effects after conditioning on depth to assess the unique contribution of the nepheloid layer beyond depth-associated gradients. All dbRDA models used 999 permutations for significance testing, with term-by-term ANOVA quantifying sequential contributions of each variable. Model R^2 values represent the proportion of community variance explained by each predictor set. For ARMS metabarcoding datasets with paired size fractions, we used restricted permutations within each ARMS to account for the non-independence of fractions collected from the same unit (Anderson 2001).

To complement variance partitioning analyses, a distance matrix approach was used to test whether community dissimilarity increased with environmental and geographic distance, providing an independent assessment of environmental filtering and dispersal limitation. These analyses use pairwise dissimilarities rather than multivariate ordination space, offering complimentary hypothesis tests less sensitive to high-dimensional structure. Environmental distance matrices were calculated as Euclidean distances between sites based on z-score standardized environmental variables. Following variable selection, for distance-based analyses, all datasets incorporated depth, turbidity, and primary productivity, while ordination and compositional analyses for ARMS metabarcoding focused on depth and turbidity only. Geographic distance matrices were calculated as least-cost distances (km) through navigable water using bathymetric data using *marmap*, (Pante & Simon-Bouhet 2013). Both environmental and geographic distance matrices were log(x+1)-transformed to improve linearity prior to analysis. Three complimentary tests using Bray-Curtis community dissimilarity matrices calculated from fourth-root transformed abundance data: (1) Simple Mantel tests assessed bivariate correlations between community dissimilarity and environmental or geographic distances using Pearson correlation with 9,999 permutations, (2) Partial Mantel tests isolated the independent effects of environmental gradients as evidence for dispersal limitation, and (3) Multiple Regression on Distance Matrices (MRM) simultaneously evaluated environmental and geographic predictors, quantifying their relative contributions via standardized regression coefficients while accounting for intercorrelation.

Taxon-Specific Responses to Environmental Gradients

Two complementary approaches were employed to identify taxa driving compositional patterns across environmental gradients, selected based on data type and taxonomic resolution. For metabarcoding datasets, we used Analysis of Compositions of Mircobiomes with Bias Correction 2 (ANCOM-BC2) implemented in the R package *ANCOMBC v 2.0.2* (Lin & Peddada 2024). ANCOM-BC2 corrects for both sample-specific (sampling fraction) and taxon-specific (sequencing efficiency) biases while controlling false discovery rates in compositional metabarcoding data. Three complementary hypotheses

were tested across datasets: (1) environmental gradient effects using continuous predictors (Depth + Turbidity for ARMS, additionally + Primary Productivity for eDNA with individual coefficient tests (global = FALSE), (2) site effects analysis identified taxa varying among the 12 sampling sites using global tests with pairwise comparisons, and (3) for ARMS datasets, size fraction effects comparing 100um, 500um, and sessile fractions. Taxa with prevalence below 10% (ARMS: prv_cut = 0.1) ot 20% (eDNA: prv_cut = 0.2) were excluded, with the stricter eDNA threshold accounting for transient DNA signals where over 50% of ASVs occurred in fewer than 5% of samples. All analyses were conducted at both phylum and family taxonomic levels, with sensitivity analysis enabled to assess robustness to pseudo-count addition in zero-inflated data. For ARMS metabarcoding (COI and 18S) environmental analyses were conducted on the full dataset and separately for motile and sessile fractions, with site effects including pairwise comparisons. For eDNA, site effects were tested without pairwise comparisons (global = TRUE, pairwise = FALSE) due to limited within-site replication and were interpreted conservatively. Significant taxa were defined using Benjamini-Hochberg adjusted p-value ($q < 0.05$), with log fold changes quantifying effect magnitudes and directions.

For count-based visual survey datasets, we used Similarity Percentage Analysis (SIMPER) implemented in vegan to identify taxa contributing most to between-group dissimilarities. SIMPER provides an interpretable decomposition of Bray-Curtis dissimilarity into individual taxon contributions, appropriate for datasets with coarser taxonomic resolution (CoralNet: 14 phyla; 2mm fauna: order-level) and smaller sample sizes (Clarke 1993). Analyses used fourth-root transformed abundance data matching the transformation applied and ordination and PERMANOVA analyses. Environmental variables (depth, turbidity) were classified into discrete groups using k-means clustering (nstart = 25) to maximize interpretability while preserving natural environmental gradients. Both binary (2 groups: low /high) and tertiary (3 groups: low /medium /high) classifications were created for each variable, allowing comparison of extreme contrast (binary) and detection of non-linear responses (tertiary). Custer assignments were ordered by environmental values to ensure biologically meaningful labels (e g., “Low” = lowest environmental values, “High” = highest values). Analyses focused on pairwise comparisons between groups, with the Low versus High contrast emphasized for reporting due to maximum environmental separation. P-values were corrected using the false discovery rate (FDR) method to account for multiple taxes tested simultaneously, with taxa passing FDR correction ($q < 0.05$) considered robust indicators of environmental associations.

Functional Feeding Group Analysis

To test whether functional feeding group predicted turbidity sensitivity, we assigned families detected in our 18S ARMS metabarcoding dataset to suspension and non-suspension functional feeding

groups based on literature review. Suspension feeders encapsulate many mechanistic categories that are subject to varying sediment tolerance and were therefore further classified into six categories reflecting sediment tolerance and particle rejection capabilities: Fine Dead-End Microfilterers (FDM), Active Dead-End Sieves (ADS), Weak Ciliary Pumpers (WCP), Truly Passive Collectors (TPC), Renewable Mucus Nets (RNM), and Ram/Crossflow feeders (RCF). Non-suspension feeders were classified as deposit feeders (DEP), predators (PRED), photoautotrophs (PHOT), grazers (GRAZ), scavengers (SCAV), or parasites (PARA) (**Table S1**). The mean log-fold change (LFC) for each functional group was calculated among families showing significant turbidity responses (ANCOM-BC2, $q < 0.05$) in the all samples dataset. To assess phylogenetic constraints on functional responses, we examined phylum-level composition within functional groups and tested for heterogeneity using variance partitioning. Suspension feeder mechanisms were compared using Welch's t-test where appropriate. Functional group composition was calculated as relative abundance at each site, ensuring values summed to 100%. Functional richness (number of groups >1% abundance) and Shannon diversity were calculated per site and tested for correlation with turbidity using Pearson's correlation. Mean functional composition was compared between sites classified as high turbidity (rank > 6) and low turbidity (rank 6).

Table S1. Classification scheme for benthic invertebrate families based on nutritional strategy. Suspension feeding groups categorized by particle capture mechanism and predicted sediment tolerance (Riisgård & Larsen 2010). Other functional groups are classified by primary nutritional mode. Functional assignments based on literature review and taxonomic expertise; families with unknown or multiple strategies classified as unclassified.

Abbreviation	Full Name	Taxa Included	Key Characteristic
Suspension Feeding Groups			
FDM	Fine Dead-End Microfilterers	All Porifera (sponges)	Pump water through fine pores; low sediment tolerance, no rejection mechanism
ADS	Active Dead-End Sieves	Bivalves, barnacles, polychaetes, copepods	Active particle sorting/rejection; moderate-high sediment tolerance
WCP	Weak Ciliary Pumpers	Bryozoans, entoprocts, brachiopods	Ciliary feeding with weak pumping; low-moderate sediment tolerance
TPC	Truly Passive Collectors	Crinoids, passive cnidarians	Flow-dependent particle capture; no active pumping
RNM	Renewable Mucus Nets	Ascidians (tunicates), Chaetopteridae	Mucus net filters regularly replaced; high sediment tolerance
RCF	Ram/Crossflow	Planktivorous fish	Ram ventilation or crossflow filtration; high tolerance
Other Functional Feeding Groups			
PHOT	Photoautotrophs	Rhodophyta (red algae) - coralline and fleshy forms	Primary production via photosynthesis; light-dependent; calcified forms sensitive to sedimentation
DEP	Deposit Feeders	Sediment ingesters across multiple phyla	Consume organic matter from sediments; surface or subsurface feeders; tolerant of high sedimentation
PRED	Predators	Active hunters across multiple phyla	Capture and consume live prey; mobile or sessile ambush feeders; opportunistic under stressed conditions
GRAZ	Grazers	Herbivores feeding on algae/biofilms	Scrape or browse algal films and macroalgae; may benefit from reduced competition at high turbidity
SCAV	Scavengers	Opportunistic feeders on detritus/carcasses	Consume dead organic matter; benefit from increased mortality at stressed sites
PARA	Parasites	Obligate parasites	Live on/in host organisms; host-specific; may increase with host stress or density

Supporting Results

Sequencing quality control

COI-ARMS (rarefied to 7,285 reads/sample) yielded 4,367 metazoan/rhodophyte ASVs across 114 samples, retaining ~80% of ASVs from the original dataset, in which 73% were successfully matched to taxonomic IDs, with 51% matched to genus level or higher. 18S-ARMS (17,000 reads/sample), retained 5,863 metazoan/rhodophyte ASVs across the same samples, with removal concentrated in rare ASVs. Taxonomic assignment was successful for 82% of these ASVs, with 46% identified to genus level.

Beta diversity and community structure

Horizontal turnover was evident in both COI- and 18S-ARMS datasets, where geographic variables explained 14-25% of community variation (PERMANOVA: $R^2 = 0.175$ for COI). Latitude and longitude contributed similarly in ARMS-based assemblages ($R^2 = 0.08$ each), whereas latitude dominated spatial patterns in 18S-eDNA communities ($R^2 = 0.12$, $p < 0.001$). Visual plate annotations showed comparable spatial differentiation, primarily along turbidity (PERMANOVA: $R^2 = 0.25$) and latitude (PERMANOVA: $R^2 = 0.21$) gradients.

Turnover patterns varied among sampling approaches. Metabarcoding datasets captured the strongest environmental structuring, with depth and turbidity jointly explaining 18-29% of community variation. However, barcoded motile macrofauna showed limited environmental coupling (PERMANOVA: $R^2 = 0.09$, $p = 0.458$) and dominant site-specific effects (PERMANOVA: $R^2 = 0.52$, $p < 0.001$). Within ARMS units, sessile fractions exhibited both higher environmental sensitivity (PERMANOVA: $R^2 = 0.28$) and spatial structuring (PERMANOVA: $R^2 = 0.26$) than motile fractions (PERMANOVA: $R^2 = 0.20$-0.27). Overall, community differentiation was shaped primarily by depth and turbidity, with spatial distance and local site effects further modulating turnover intensity across datasets and functional groups.

Primary productivity structured ARMS and eDNA communities through subtle but widespread effects, with 69 families (30% of total effects) responding to the oligotrophic western to eutrophic eastern Gulf gradient (median LFC = 0.004, all $q < 0.05$). Rhodymeniaceae declined with productivity (LFC = -0.017, $q = 8.8\times10^{-10}$), while bioeroding Clionaidae (LFC = 0.032, $q = 3.4\times10^{-8}$) and Salpidae (LFC = 0.0028, $q = 7.6\times10^{-6}$) increased. Among molluscs, Mytilidae (LFC = -0.0042, $q = 1.4\times10^{-6}$) and Calyptraeidae (LFC = -0.0082, $q = 9.0\times10^{-6}$) declined with productivity. Fifty families responded to multiple gradients simultaneously, with 15 families responding to all three predictors (depth, turbidity, productivity), indicating complex niche structuring beyond single-axis environmental filtering. Barcoded 2mm macrofauna exhibited minimal taxon-specific environmental associations compared to sessile communities. Only one order (Valvatida) showed significant turbidity association after FDR correction

(5.1-fold higher in turbid water, p_FDR = 0.04), despite strong community-level environmental structure in ordination analyses. This pattern contrasted fundamentally with sessile CoralNet communities, which exhibited seven phyla with significant taxon-environment associations (p_FDR < 0.05). The disparity suggests mobile organisms can behaviorally select microhabitats or avoid unfavorable conditions, decoupling individual taxon distributions from environmental gradients, while sessile organisms remain constrained by local abiotic conditions.

Weak ciliary pumpers (WCP) showed no consistent trend and deposit feeders remained stable. Unclassified taxa comprised 30-42% of communities, reflecting incomplete trait coverage but distributed evenly across the turbidity gradient.

Supporting Discussion

Environmental filtering as the primary driver of metacommunity structure

Our measurements of turbidity captured the influence of the benthic nepheloid layer, a well-documented oceanographic feature of the TX-LA continental shelf, characterized by elevated suspended sediment concentrations near the seafloor (Shideler, 1981; McGrail & Carnes, 1983; Rezak et al., 1990). This persistent turbid layer can reach thicknesses of up to 35 m along the shelf edge (Shideler, 1981), creating a strong environmental gradient that varies spatially across our study area and directly impacts benthic communities through multiple mechanisms. This study extends previous work on the biotic zonation patterns of historical descriptions of community structure on these banks in relation to nepheloid layer dynamics (Rezak *et al.* 1985, 1990; Sammarco *et al.* 2016). Previous research has shown that the intensity and persistence of the nepheloid layer varies considerably across the TX-LA shelf, with banks closest to shore and at intermediate depths often experiencing the most severe and chronic turbidity stress (Rezak *et al.* 1990; Tunnell 2007). Our observed latitudinal gradient in turbidity effects aligns with these documented patterns, where northward intensification of the nepheloid layer has been linked to proximity to terrigenous sediment sources and shelf-scale circulation patterns (Dennis & Bright 1988; Mcgrail & Carnes 1983).

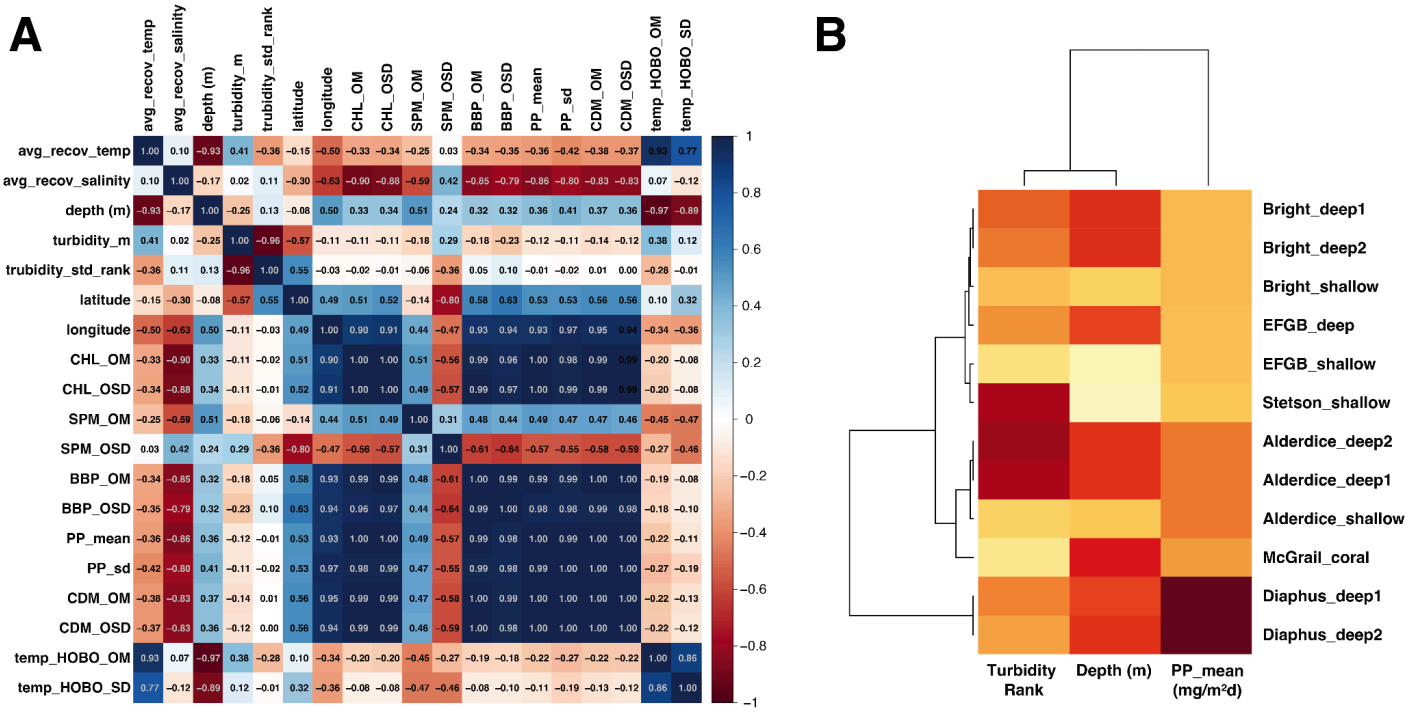

Figure S1. Environmental variable correlation and site clustering based on key parameters from ARMS deployments. (A) Correlation matrix of 19 environmental variables measured or derived from in-situ loggers, diver observations, and satellite data. Color intensity represents correlation strength, with dark blue indicating strong positive correlations (1.0) and dark red indicating strong negative correlations (-1.0). Several oceanographic parameters show strong intercorrelation, particularly between chlorophyll-a (CHL), backscattering coefficient (BBP), and primary productivity (PP). B) Hierarchical clustering of 12 sampling sites based on three environmental variables: Turbidity Rank, Depth (m), and Primary Production (PP_mean, mg/m²d). Color intensity indicates scaled variable values, with yellow representing low values and dark red representing high values. The dendrogram on the left illustrates the hierarchical clustering of sites based on environmental similarity.

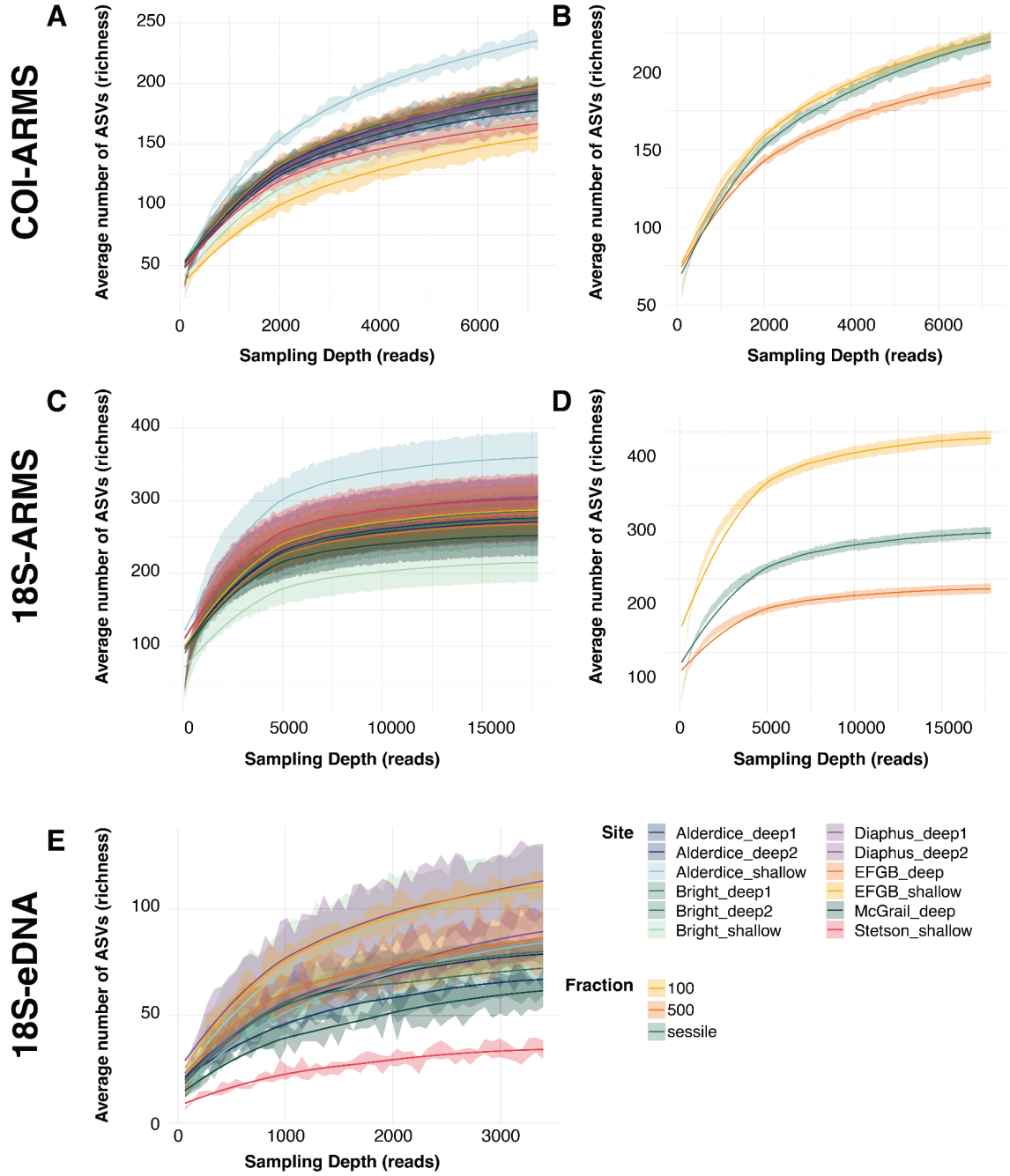

Figure S2. Comparison of metabarcoding biodiversity sampling techniques showing relationship between sequencing depth (reads) and ASV richness across different bank sites and size fractions. (A) COI-ARMS rarefaction curves by site (B) and size fraction. (C) 18S-ARMS rarefaction curves by site (D) and size fraction. (E) 18S-eDNA rarefaction curves by site. Shaded areas represent confidence intervals around each curve.

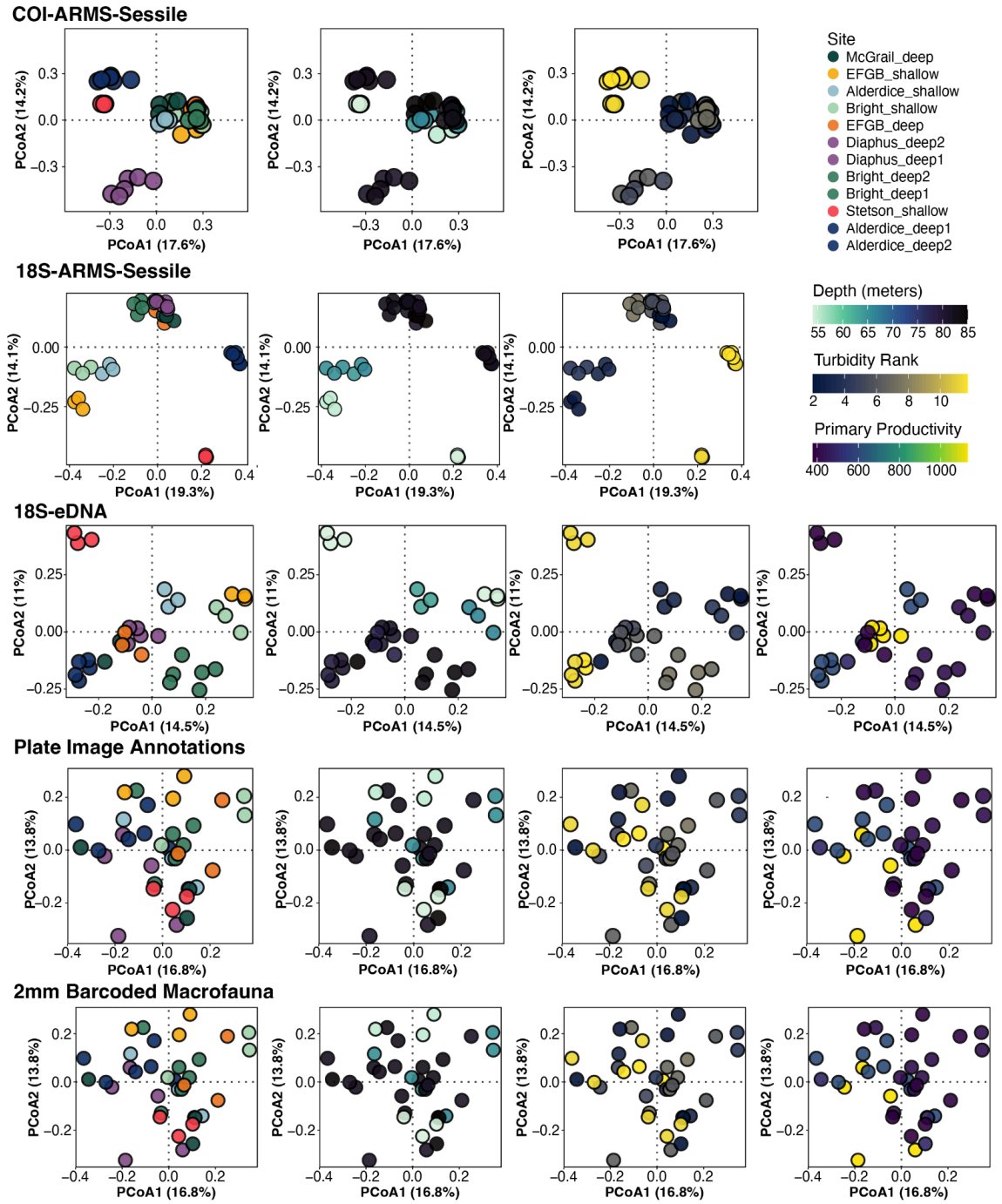

Figure S3. Principal Coordinates Analysis (PCoA) of marine community composition across different biodiversity assessment methods, colored by environmental gradients. Ordination plots are arranged by assessment method (rows: COI-ARMS-Sessile, 18S-ARMS-Sessile, 18S-eDNA, Plate Image Annotations, 2mm Barcoded Macrofauna) and colored by different environmental variables (columns: sampling site, depth in meters, turbidity rank, and primary productivity). Points represent individual samples, with closer points indicating more similar community composition. Numbers in parentheses along axes represent the percentage of total variation explained by each PCoA axis. The analysis is based on Bray-Curtis dissimilarity matrices derived from the same dataset used in previous NMDS analyses.

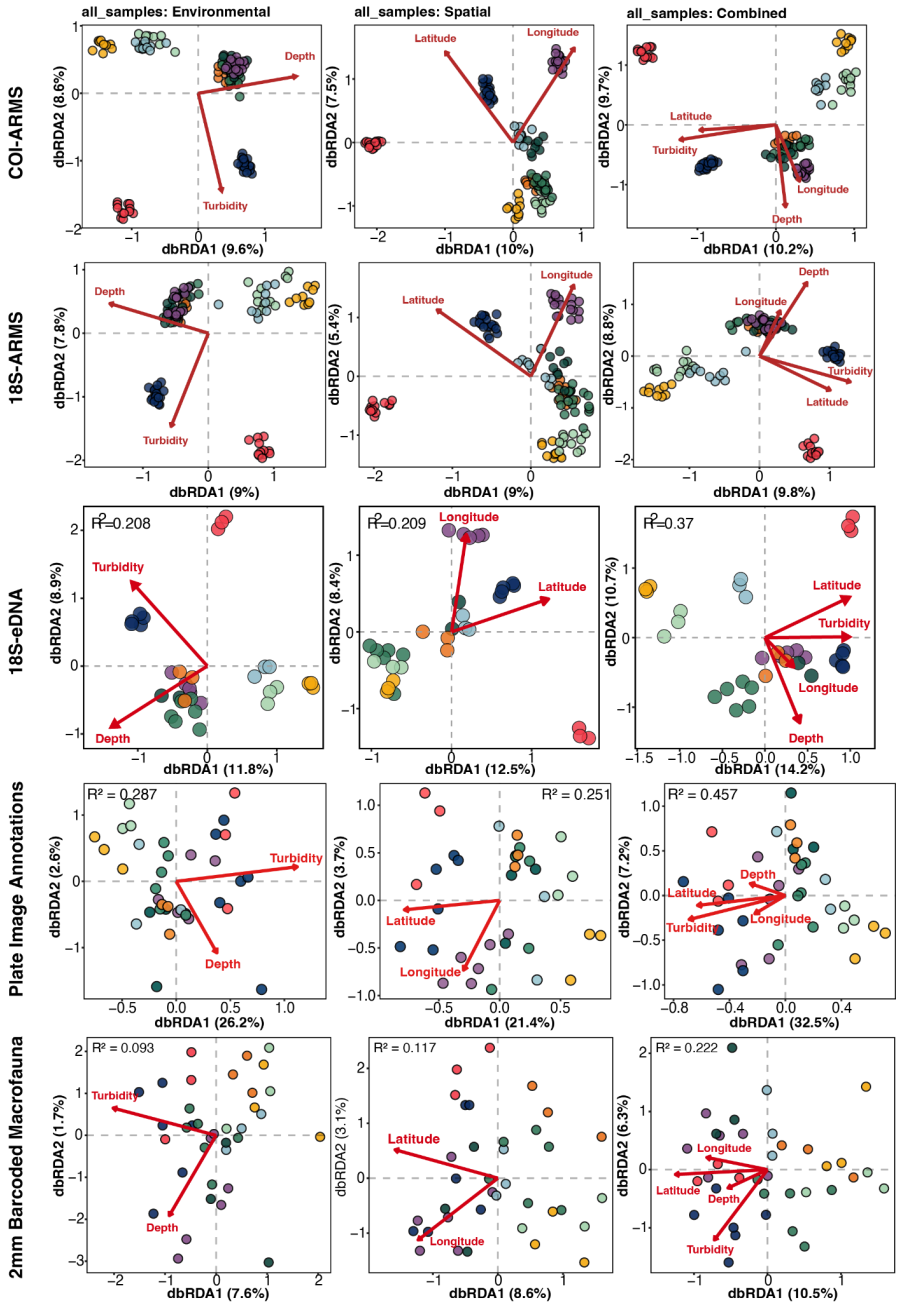

Figure S4. Distance-based redundancy analysis (dbRDA) showing the influence of environmental and spatial variables on marine community composition across different biodiversity assessment methods. Ordination plots are arranged by assessment method (rows: COI-ARMS, 18S-ARMS, 18S-eDNA, Plate Image Annotations, Motile Fauna) and explanatory variable groups (columns: Environmental, Spatial, Combined). Environmental models include depth and turbidity vectors, spatial models include latitude and longitude vectors, and combined models incorporate all four variables. Points are colored by sampling site. Red vectors indicate the direction and strength of each explanatory variable's influence on community structure. Numbers in parentheses along axes represent the percentage of total variation explained by each dbRDA axis. R^2 values indicate the proportion of community variation explained by the respective model.

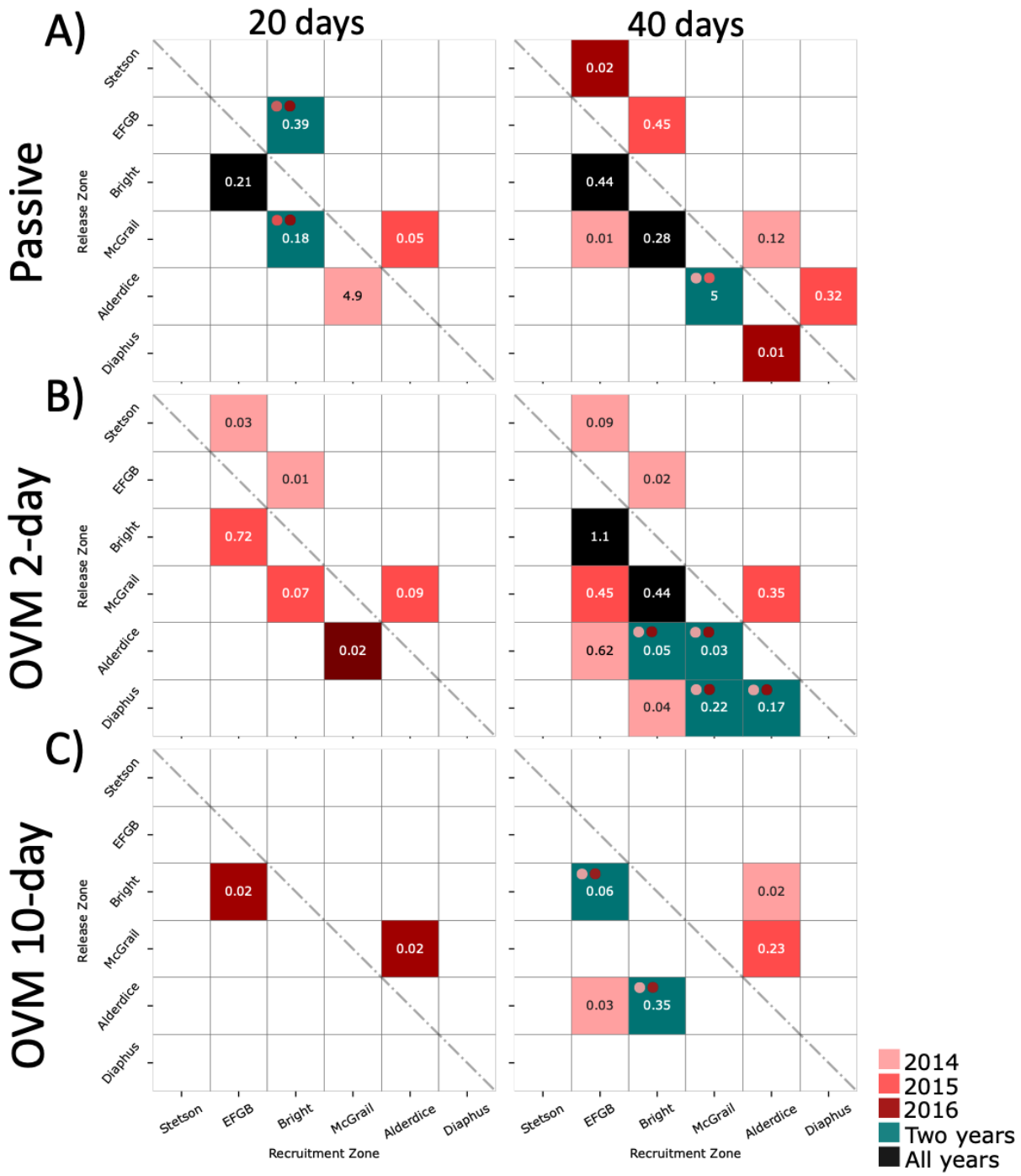

Figure S5: Ensemble connectivity matrices from 2014 to 2016 for both 20 and 40 transport durations: (A) Passive scenario, (B) OVM 2-day, (C) OVM 10-day. The color scale indicates the year(s) when the connection occurred. Pink-to-magenta colors represent individual years (2014, 2015, or 2016); blue indicates connections occurring in two years, with the dots above specifying which years; and black indicates connections present in all three years.

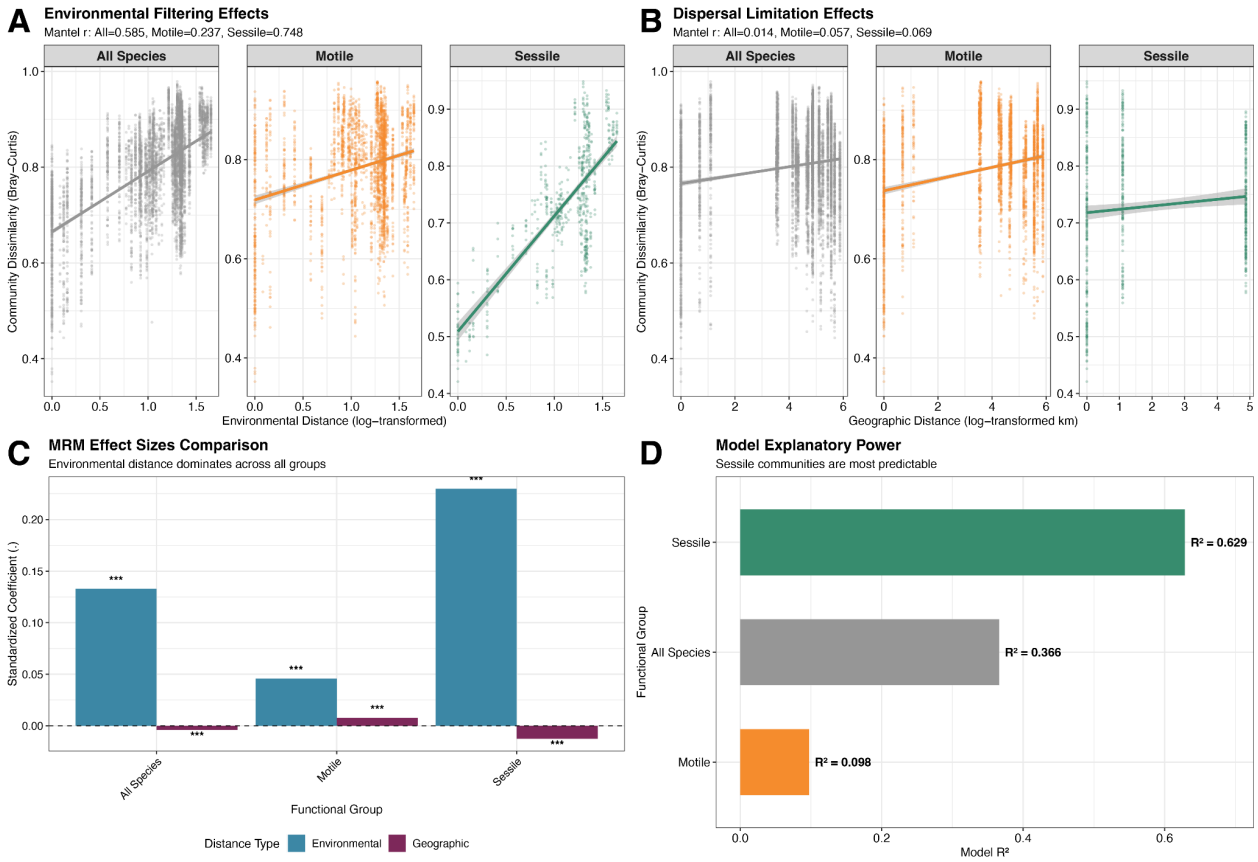

Figure S6. Distance-based analyses of 18S rDNA metabarcoding communities across functional groups. Relationship between environmental and geographic distances with community structure. (A) Environmental distance (log-transformed) plotted against community dissimilarity (Bray-Curtis) for all species, motile, and sessile communities with corresponding Mantel correlation coefficients. (B) Geographic distance (log-transformed km) plotted against community dissimilarity for the same community groups with corresponding Mantel correlation coefficients. (C) Standardized coefficients from Multiple Regression on distance Matrices (MRM) showing relative magnitude of environmental (blue) and geographic (purple) effects for each functional group. (D) Model R^2 values from combined environmental and geographic MRM models for each functional group. Asterisks indicate statistical significance levels.

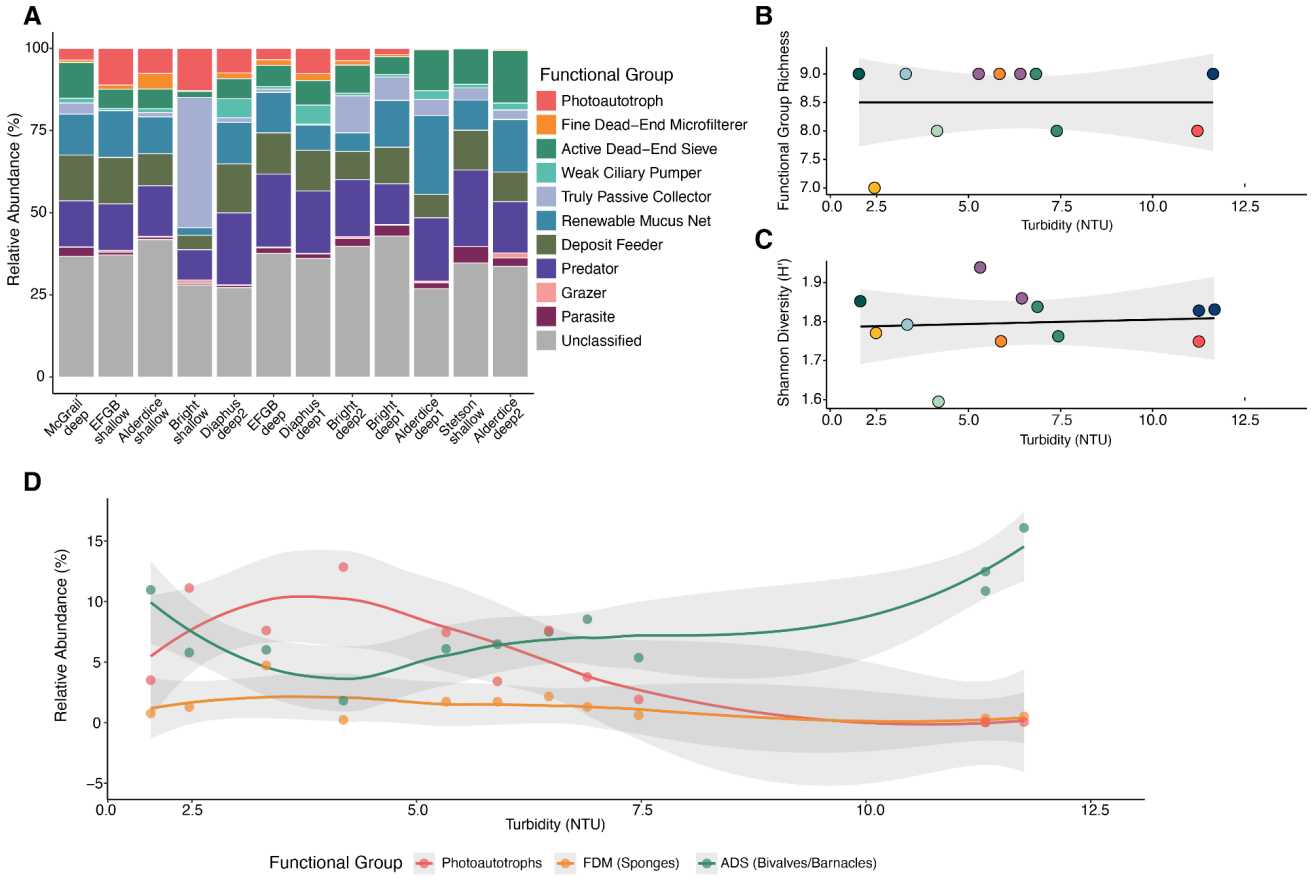

Figure S7. Family-level functional group composition across 12 ARMS sites based on 18S metabarcoding . (A) Stacked bar plot showing relative abundance (%) of functional groups based on 18S metabarcoding (n = 359 families, 83% assigned functional traits) across 12 ARMS sites. Sites are ordered left to right by decreasing turbidity (high to low). Grey portions represent families lacking trait assignments. Colors indicate different functional groups including photoautotrophs (red), fine dead-end microfilterers (FDM; orange, primarily sponges), and active dead-end sieves (ADS; green, primarily bivalves and barnacles). (B) Scatter plot displaying functional group richness (number of groups >1% abundance) against turbidity gradient. Points are colored by site identity. (C) Scatter plot of Shannon functional diversity index (H') versus turbidity gradient, with points colored by site identity. (D) Line graph showing relative abundance of three key functional groups (photoautotrophs, FDM, and ADS) plotted against turbidity. LOESS smoothers with 95% confidence intervals are displayed for each group.

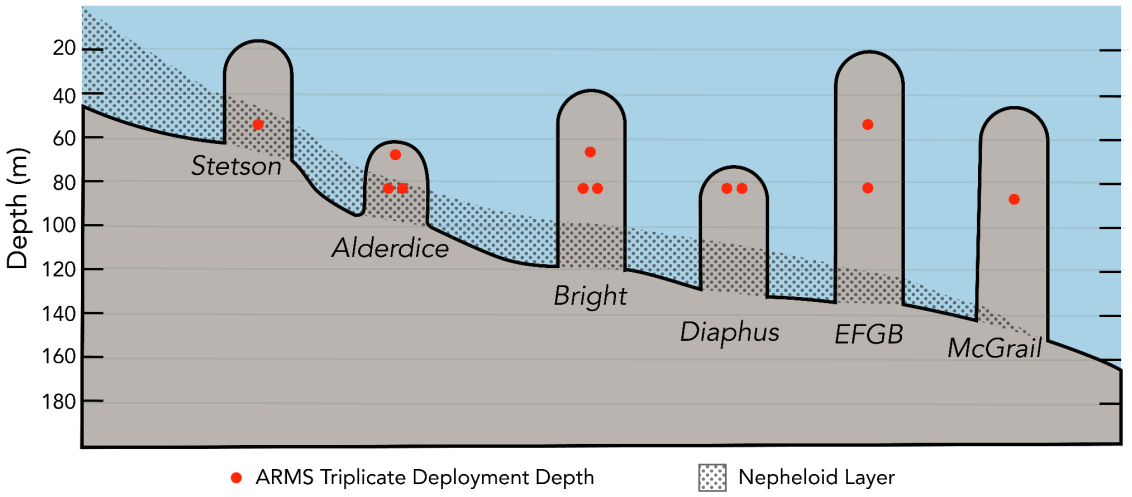

Figure S8. **Schematic cross-section of study banks and approximate nepheloid layer distribution on the TX-LA continental shelf.** Stippled area represents nepheloid layer distribution, with red dots indicating ARMS deployment depths at each bank. Figure modified from Rezak et al. 1990 (Rezak *et al.* 1990).

Table S2. Environmental conditions at ARMS deployments sites over the two-year study period. Mean temperature (ºC), light intensity (lux), and dissolved oxygen (DO, mg/L) measurements y in-situ data loggers attached one ARMs per triplicate. Temperature was measured at all sites, while light intensity (reported with and without zero values included) and dissolved oxygen were recorded at select location. Standard deviations (STD) indicate temporal variability over the deployment period. Missing data indicated by dashes (-).

Site	Mean Temp (ºC)	Temp STD (ºC)	Mean Lux (nonzeros)	Lux STD (nonzeros)	Mean Lux (zeros)	Lux STD (zeros)	Mean DO (mg/L)	DO STD (mg/L)
Stetson shallow	22.143	2.084	36.003	38.677	1.362	10.189	-	-
EFGB deep	20.763	1.106	-	-	-	-	-	-
EFGB shalllow	22.554	1.693	-	-	-	-	-	-
Bright shallow	21.648	1.209	69.147	108.744	15.384	58.815	-	-
Bright deep1	20.606	0.704	-	-	-	-	6.091	0.781
Bright deep2	20.737	0.957	-	-	-	-	-	-
McGrail deep	20.622	0.917	-	-	-	-	-	-
Alderdice deep1	20.749	0.930	-	-	-	-	6.059	0.629
Alderdice deep2	20.668	0.907	-	-	-	-	-	-
Alderdice shallow	22.073	1.312	86.022	117.390	18.605	66.865	-	-
Diaphus deep1	20.993	1.205	-	-	-	-	-	-
Diaphus deep2	20.972	1.184	-	-	-	-	6.567	0.910